STUK

STUK-YTO-TR 156 May 1999

ON GROUNDWATER FLOW MODELLING IN SAFETY ANALYSES OF SPENT FUEL DISPOSAL

A comparative study with emphasis on boundary conditions

Petri Jussila

In STUK this study was supervised by **Esko Eloranta**

STUK • SÄTEILYTURVAKESKUS • STRÅLSÄKERHETSCENTRALEN
RADIATION AND NUCLEAR SAFETY AUTHORITY

The conclusions presented in the STUK report series are those of the author and do not necessarily represent the official position of STUK.

ISBN 951-712-304-3
ISSN 0785-9325

Oy Edita Ab, Helsinki 1999

JUSSILA, Petri. On groundwater flow modelling in safety analyses of spent fuel disposal. A comparative study with emphasis on boundary conditions. STUK-YTO-TR 156. Helsinki 1999. 42 pp. + Appendices 27 pp.

ISBN 951-712-304-3
ISSN 0785-9325

Keywords: groundwater flow, modelling, spent fuel disposal, boundary conditions

ABSTRACT

Modelling groundwater flow is an essential part of the safety assessment of spent fuel disposal because moving groundwater makes a physical connection between a geological repository and the biosphere. Some of the common approaches to model groundwater flow in bedrock are equivalent porous continuum (EC), stochastic continuum and various fracture network concepts. The actual flow system is complex and measuring data are limited. Multiple distinct approaches and models, alternative scenarios as well as calibration and sensitivity analyses are used to give confidence on the results of the calculations. The correctness and orders of magnitude of results of such complex research can be assessed by comparing them to the results of simplified and robust approaches.

The first part of this study is a survey of the objects, contents and methods of the groundwater flow modelling performed in the safety assessment of the spent fuel disposal in Finland and Sweden. The most apparent difference of the Swedish studies compared to the Finnish ones is the approach of using more different models, which is enabled by the more resources available in Sweden. The results of more comprehensive approaches provided by international co-operation are very useful to give perspective to the results obtained in Finland.

In the second part of this study, the influence of boundary conditions on the flow fields of a simple 2D model is examined. The assumptions and simplifications in this approach include e.g. the following:

- the EC model is used, in which the 2-dimensional domain is considered a continuum of equivalent properties without fractures present,
- the calculations are done for stationary fields, without sources or sinks present in the domain and with a constant density of the groundwater,
- the repository is represented by an isotropic plate, the hydraulic conductivity of which is given fictitious values,
- the hydraulic conductivity of rock is supposed to have an exponential depth dependence,
- the elevation of the water table is fixed and varies with the topography of the ground surface.

The calculations are performed with the aid of Matlab® Partial Differential Equation Toolbox, whose approach to create meshes and to do the calculations are not looked into in this study.

When selecting a location for a repository, the interest would be to find conditions, where the flow through the repository is small and directed away from the biosphere. According to the results of the simple model, favourable features for the system are e.g. a small variation of the absolute value and a high frequency of the regional variation of the elevation of the water table (i.e. the ground surface), small conductivity of the repository and the location of the repository under a hill. The influence of a repository on the flow pattern is small, especially when some or all of the conditions above are true. Furthermore, the changes concentrate in the vicinity of the repository. In the cases considered in the study, the influence of the variation of the boundary conditions on the sides and at the bottom of the modelling domain on the flow pattern in the vicinity of the repository is small.

JUSSILA, Petri. Pohjaveden virtausmallinnuksesta käytetyn polttoaineen loppusijoituksen turvallisuusanalyyseissä. Vertaileva tutkimus korostaen reunaehtojen asettamista. STUK-YTO-TR 156. Helsinki 1999. 42 s. + liitteet 27 s.

ISBN 951-712-304-3
ISSN 0785-9325

Avainsanat: pohjavesivirtaus, mallintaminen, käytetyn ydinpolttoaineen loppusijoitus, reunaehdot

TIIVISTELMÄ

Pohjavesivirtauksen mallintaminen on käytetyn ydinpolttoaineen loppusijoituksen turvallisuusarvioinnin keskeinen tutkimusalue, sillä liikkuva pohjavesi muodostaa yhteyden biosfäärin ja geologisen loppusijoitustilan välille. Ekvivalentin huokoisen jatkumon (EC-malli) ja stokastisen jatkumon mallit sekä lukuisat erilaiset rakoverkkomallit ovat eräitä tyypillisiä tapoja kuvata kallioperää pohjavesivirtauksen väliaineena. Todellinen virtausjärjestelmä on hyvin monimutkainen ja mittaustulokset ovat puutteellisia. Useita erillisiä lähestymistapoja ja malleja, vaihtoehtoisia skenaarioita sekä kalibrointia ja herkkyysanalyysejä käytetään lisäämään varmuutta laskujen antamiin tuloksiin. Monimutkaisen tutkimuksen antamien tulosten oikeellisuutta ja suuruusluokkia voidaan arvioida vertaamalla niitä yksinkertaisempien, ”robustien” mallien antamiin tuloksiin.

Tämän työn ensimmäinen osa on kirjallisuuskatsaus Suomessa (VTT) ja Ruotsissa (SKI) tehtyjen loppusijoitustutkimuksiin liittyvien pohjavesivirtausmallinnusten tavoitteisiin, sisältöihin ja menetelmiin. Ruotsalaisten tutkimusten näkyvin ero suomalaisiin verrattuna on suurempien resurssien mahdollistama käytäntö hyödyntää useampia eri malleja. Suomessa tehtävä suppeampi tutkimus hyötyy kansainvälisestä yhteistyöstä, joka tarjoaa monipuolisempiin lähestymistapoihin pohjautuvia kokemuksia ja tuloksia.

Tämän työn toisessa osassa tarkastellaan reunaehtojen vaikutusta yksinkertaisen mallin mukaisiin virtauskenttiin tasotapauksessa. Käytetyn mallin oletuksia ja yksinkertaistuksia ovat mm. seuraavat:

- virtaussysteemiä kuvataan EC-mallilla, missä 2-ulotteinen mallinnusalue oletetaan ekvivalentiksi jatkumoksi ilman rakoja,
- lasketut tapaukset ovat stationaarisia, mallinnusalueessa ei ole lähteitä eikä nieluja ja pohjaveden tiheys on vakio,
- loppusijoitustilaa mallinnetaan isotrooppisella levyllä, jonka vedenjohtavuudelle annetaan kuvitteellisia arvoja,
- kallion vedenjohtavuudelle oletetaan eksponentiaalinen syvyysriippuvuus,
- pohjaveden pinta on kiinnitetty ja mukailee maanpinnan korkeutta.

Laskuissa käytetään apuna Matlab®-ohjelmiston Partial Differential Equation Toolbox –työkalua, jonka laskentaverkon muodostamistapaan ja laskentatapaan ei tutustuta yksityiskohtaisesti.

Loppusijoitustilan sijainnin toivottavia ominaisuuksia pohjaveden liikkeen kannalta ovat mm. vähäinen virtaus tilan läpi ja virtauksen suuntautuminen poispäin biosfääristä. Työssä käytetyn yksinkertaisen mallin antamien tulosten perusteella näille ehdoille suotuisia tapauksia ovat esim. pohjaveden korkeuden (eli maanpinnan korkeuden) tiheä vaihtelu ja vähäiset absoluuttiset korkeuserot, loppusijoitustilan pieni vedenjohtavuus ja loppusijoitustilan sijainti mäen alapuolella. Loppusijoitustilan vaikutus virtauskenttään on vähäinen, varsinkin jos yksi tai useampi edellä luetelluista ehdoista toteutuu. Lisäksi aiheutuneet muutokset rajoittuvat sijoitustilan lähiympäristöön. Mallinnusalueen sivuilla ja pohjalla vallitsevien reunaehtojen vaihtelun vaikutus virtauskenttään loppusijoitustilan ympäristössä on työssä käsitellyissä tapauksissa vähäinen.

CONTENTS

1 INTRODUCTION

Understanding the stability of the passive films forming on copper is of great importance when considering the use of copper as an outer shield of cast iron canisters for storage of spent nuclear fuel. The copper shield is responsible for the corrosion protection of the canister construction. Nitrites, chlorides, sulphides and carbonates have been suggested to affect the stability of the oxide films on copper and to promote localised corrosion. However, a consistent model for the growth and stability of copper oxide films has not been available, which has made a mechanistic understanding of the influence of these detrimental anions difficult.

On the basis of our previous experimental work, the oxide film formed on Cu in $Na_2B_4O_7$ solutions at 80 °C was depicted as consisting of a conductive layer and a very thin semiconductive layer. The aim of the present work is to study and discuss the influence of bicarbonate (HCO_3^-) anions on the stability of the copper oxide film. The work consists of a brief literature survey and an experimental part, in which voltammetry, electrochemical impedance spectroscopy and dc resistance measurements via the Contact Electric Resistance (CER) technique were used as the main techniques.

2 LITERATURE SURVEY

Electrochemical measurements in slightly alkaline solutions have shown that the passivation of the copper surface involves the formation of cuprous oxide and cupric oxide together with cupric hydroxide surface compounds. Above a certain threshold potential, which depends largely of the solution composition and pH, the breakdown of the oxide film and the initiation of copper pitting has been reported [1]. The electrochemical behaviour of Cu in alkaline solutions is rather complex, but some information about the relative contributions of all these reactions has been obtained by performing voltammetric measurements.

2.1 Voltammetric studies

Voltammetric measurements can be used not only to obtain an overview of the electrochemical behaviour of the studied material at different potentials, but also to obtain preliminary kinetic information about the reactions occurring on the metal surface. The polarisation curves of copper in bicarbonate solutions can be divided into four different sections as shown in Fig. 1a.

Section I consists of the first anodic current peak, which is followed by the passivation of the copper surface in section II. According to Drogowska et al. [29], these two regions are connected to the formation of an inner Cu_2O layer of the oxide film according to the reaction below.

$$2\,Cu + H_2O = Cu_2O + 2H^+ + 2\,e^- \quad (1)$$

Drogowska et al. made also a measurement in which they formed the oxide film on the copper surface in the upper part of the section II and then reduced it. The measured Q_{red}/Q_{ox} ratio was found to be close to 1, indicating that no soluble species are released to the solution during the formation of an oxide film in the region of monovalent copper. Furthermore, they reported that the formation of cuprous oxide is thermodynamically as well as kinetically more likely than the formation of copper carbonates. The authors reported also that with increasing temperature the height of the first anodic peak increases and the potential shifts to more negative values [2].

Section III comprises the second anodic peak and a broad oxidation area where the current is independent of the potential. The possible reactions occurring in this region can be written as:

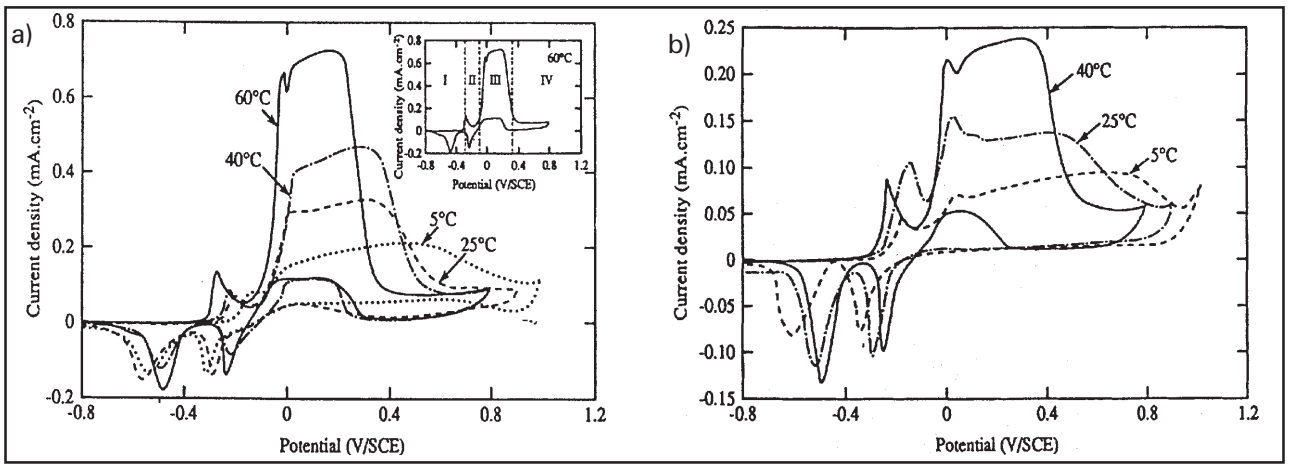

Fig. 1. *(a) Cyclic voltammograms for a Cu disc electrode rotated at 1000 rpm, sweep rate of 5 mVs^{-1} at 5, 25, 40 and 60 °C* ***a)****: in 0.1 m $NaHCO_3^-$ solution (pH 8),* ***b)****: in a 0.05 m $NaHCO_3$ solution (pH 8) [2].*

$$Cu_2O + H_2O = 2CuO + 2\,H^+ + 2\,e^- \quad (2)$$

$$Cu_2O + 3H_2O = 2\,Cu(OH)_2 + 2\,H^+ + 2\,e^- \quad (3)$$

and

$$Cu_2O + 2HCO_3^- = 2CuCO_3 + H_2O + 2\,e^- \quad (4)$$

$$CuCO_3 + HCO_3^- = [Cu(CO_3)_2]^{2-} + H^+ \quad (5)$$

Within Section III passive film is growing and may compose of copper carbonates, whose structure can approach that of malachite ($CuCO_3$*$Cu(OH)_2$) or azurite ($2CuCO_3$*$Cu(OH)_2$) if the pH of the solution is higher than 10.5. Malachite can react with bicarbonate ions forming highly soluble copper complex ions through reactions (6) and (7).

$$CuCO_3*Cu(OH)_2 + HCO_3^- = 2\,[Cu(CO_3)_2]^{2-} + 2\,H_2O + H^+ \quad (6)$$

$$CuCO_3*Cu(OH)_2 + HCO_3^- = 2\,[Cu(CO_3)(OH)_2]^{2-} + H^+ \quad (7)$$

On the other hand, copper carbonates ($CuCO_3$) as such or Cu(I) carbonate complexes have not been detected nor reported [2,3].

The temperature influences significantly the broad oxidation region in Section III as shown in Fig. 1. The figure clearly shows that the anodic currents increase with increasing temperature. The authors reported also that the reduction efficiency during the negative going sweeps fell from 100% to 11 % with increasing temperature. Interaction between bicarbonate and Cu(II) ions resulting in soluble complexes may explain the observed, significantly different anodic behaviour of copper in solutions containing bicarbonates compared to that of other aqueous electrolytes. In the absence of carbonates, Cu(II) compounds on the copper surface assured an extensive range of passivity [3,4].

Section IV in Fig. 1 shows the secondary passivation of the copper electrode surface before oxygen evolution begins. Increasing temperature narrows the second oxidation region (Section III) and reciprocally makes the secondary passivation region wider as shown in Fig. 1a. Drogowska et al. have reported this to result from increased copper dissolution-precipitation rate with temperature. Furthermore, the temperature increase of the bicarbonate solution increases the amount of current flowing through the oxide film. This suggests that the film becomes less protective towards general corrosion [3,4].

The typical reduction peaks of CuO and Cu_2O are detected during the negative going sweeps. Several authors have reported also an anodic current peak during the reverse sweep. A clear anodic peak can be seen during the reverse sweep in Figs 1 and 2 roughly between $-0.2\ V < E < 0.3\ V$. This has been reported to be an indication of the reactivation of the electrode surface despite of the fact that the surface remained covered with Cu_2O film [3–5].

In addition to temperature, the electrolyte flow rate has an effect on the shape of the voltammograms. Stirring does not affect significantly the height of the first anodic peak whereas the sections II and III seem to be remarkably dependent on hydrodynamics. This indicates that the rate of base metal electrodissolution process is promoted by chemical dissolution of the passivating surface layer [1,3,5]. When the stirring and pH is kept constant and concentration of HCO_3^- increased, the measured anodic currents are higher i.e. the amount of soluble Cu(II) species in the solution increases [3].

2.2 Effect of bicarbonate concentration and pH on passive film on copper surfaces

Thomas et al. [6,7] have shown that in air-saturated solutions at ambient temperature the oxide film formed on copper is protective in 0.01 m $NaHCO_3$. Nevertheless, at high enough positive potentials the oxide film broke down and high currents were measured. This supports again the idea that a possible breakdown occurs through the reaction with cupric hydroxide film rather than the cuprous oxide film as indicated in the previous chapter. Thus the oxide films with different valency formed on the copper surface exhibit different characteristics towards anions.

As the bicarbonate concentration is increased, the oxide film is less protective towards general corrosion, probably due to the increasing formation of soluble copper carbonate complexes. This

increasing solubility of copper complexes explains the measured increasing corrosion currents through the cuprous oxide film with increasing bicarbonate concentration as shown in Fig. 1 [2]. The results suggest that the bicarbonate ions do not interfere with Cu_2O formation, but Cu^{2+} ions are stabilised by the complexing action of HCO_3^-. This was confirmed by the observation that a higher bicarbonate anion concentration caused an increase in the anodic current, but the cathodic currents were not significantly affected

The estimated oxide thickness on the copper samples depended only slightly on the electrolyte concentration (0.1–0.001 M $NaHCO_3$) but depended mostly on the time the sample was kept at each potential. A more significant change in the film thickness was observed as the temperature was increased from 5 to 60 °C (from 1.6 nm to 4.6 nm, respectively) [2].

Not only the bicarbonate concentration but also the pH of the solution affects the breakdown of the oxide film and the pitting phenomena on copper surfaces. The anodic behaviour of copper in dilute $NaHCO_3$ solutions (pH 8) indicates that corrosion proceeds at localised areas rather than in pits and continues as a quasi-homogeneous Cu dissolution through the anodic film [2]. Behaviour of the copper surface is different if the carbonate concentration is increased. The voltammograms of copper in two bicarbonate solutions with two different pH-values are shown in Fig. 2. According to Sanchez et al. the pitting potential of copper is 0.4 V vs. SCE at pH 8.7 and 0.53 V vs. SCE at pH 11. They reported that a number of current fluctuations were measured in the voltammogram at potentials more positive than 0.4 V vs. SCE as shown in Fig. 2 [1]. Typically these fluctuations are related to partial breakdown and reforming of the oxide film.

Sanchez et al. investigated copper surfaces with SEM after potential cycling of the specimens. They found out that in 0.1 m $NaHCO_3$ solutions a milder pitting corrosion and much lower pit density was observed on the surfaces than when the samples were exposed to solution with higher pH-value. On the other hand, as the potential sweep was reversed before the pits were observed, no clear Cu pitting was established and the measurements showed a nearly homogeneous copper electrodissolution through the anodic layer.

The increasing amount of soluble Cu(II) species with higher concentration of carbonate ions in the solution generated by reactions (5),(6) and (7) could be explained by the increase in the HCO_3^- surface concentration [1]. Sanchez et al. stated that for the $NaCO_3$+$NaHCO_3$ solutions the local acidification implies a local increase in the concen-

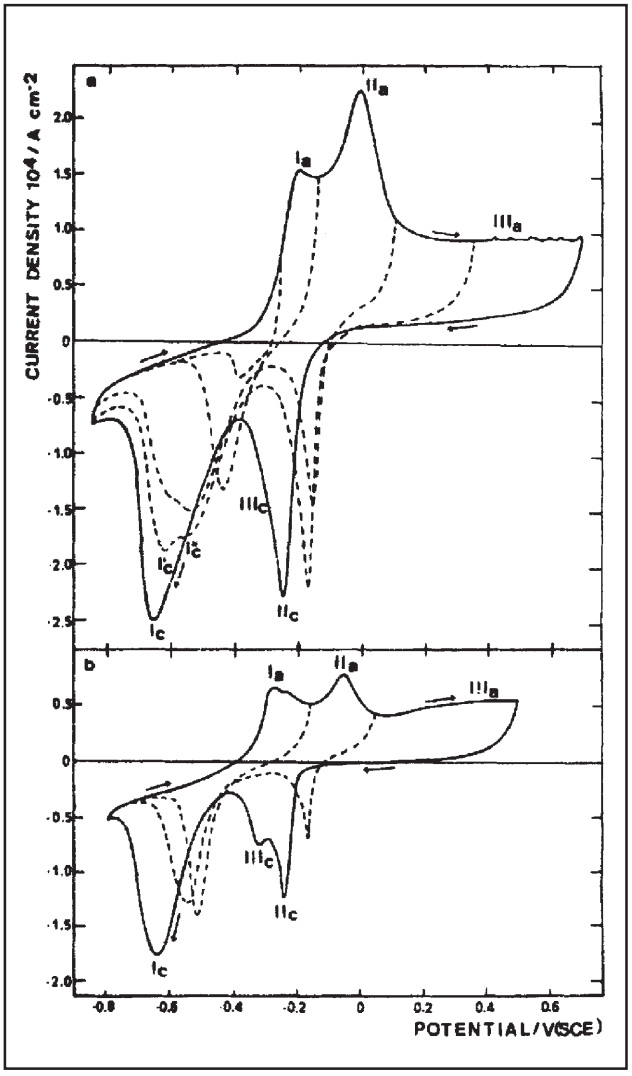

Fig. 2. *Voltammogramms of copper in $NaHCO_3$ + Na_2CO_3 solutions at 10 mVs-1: a) 0.09 m $NaHCO_3$ + 0.01 m Na_2CO_3, pH 9.1; b) 0.03 m $NaHCO_3$ + 0.07 m Na_2CO_3, pH 11 [1].*

tration of HCO_3^- ion in such a way that it should be considered as the actual aggressive ion for Cu pitting. This fact explains the pH dependence of the pitting potential [1].

Ribotta et al. [3] stated that in lower pH solutions HCO_3^- behaves as an aggressive ion, but with increasing solution pH the total dissolution rate of the base metal is determined by the combined effects of bicarbonate and pH of the solution. This implies that with low pH value and high carbonate concentration in the solution, pitting is observed on the copper surface. On the other hand, the surface is less prone to experience pitting when carbonate concentration is low in low or high pH solutions [3,8].

2.3 Comments on the relevance of the test environments

Despite the great importance of bicarbonates in copper corrosion, most of the environments used in the electrochemical and corrosion studies are not comparable with repository conditions. In the existing studies either the bicarbonate concentrations or pH of the solutions are too high. In addition, no such studies are available in which not only the effect of carbonate ions, but also possible synergetic effects of these species with other aggressive ions would have been clarified. The joint actions of different ions are theoretically extremely difficult to model.

3 EXPERIMENTAL PART

The experimental part was focused on finding possible evidence of local damage to the oxide films on copper in the presence of bicarbonate ions.

3.1 Materials, experimental conditions and equipment

Phosphorus microalloyed copper (Cu OFP) containing 99.992 wt-% Cu and 45 ppm P (Outokumpu Poricopper Oy) was used as the test material in all the experiments. The experiments were performed in a static titanium cladded autoclave. The electrolyte was deaerated and pressurised to 2 MPa using a mixture of Ar+3% H_2. The working electrodes were polished using 4000 grit emery paper and rinsed with MILLI-RO® 15 water before use. A Pd electrode saturated with hydrogen was used as a reference and was assumed to behave as a Reversible Hydrogen Electrode (RHE). All the potentials in this work are reported on the reversible hydrogen electrode scale. The solutions were made of p.a. $Na_2B_4O_7$, p.a. $NaHCO_3$ and MILLI-RO® 15 purified water. The CER equipment was supplied by Cormet Ltd. Potentiostatic and potentiodynamic conditions were ensured using a Wenking LB 81M potentiostat and a Hi-Tek Instruments PPR1 waveform generator. Voltammetric and impedance measurements were performed by a Solartron ECI 1287/FRA 1260 system controlled by ZPlot / CorrWare software (Scribner) in a frequency range 0.01 Hz...10 kHz at an AC amplitude of 10 mV (rms). Capacitance vs. potential curves were registered at a sweep rate of 1 mVs^{-1} and a frequency of 970 Hz.

3.2 Results and discussion

3.2.1 Voltammetric behaviour

A cyclic voltammogram of Cu OFP in 0.1 M $Na_2B_4O_7$ +1.7 mM HCO_3^- is shown in Fig. 3a. The shape of the curve is qualitatively similar to that measured in pure 0.1 M $Na_2B_4O_7$ [9], except for the anodic excursion observed during the negative going sweep in the potential range 1.0…0.65 V.

The currents measured during negative going potential sweeps after different oxidation times at different potentials are shown in Figs 3b…4b. The potential 0.6 V corresponds to the stability region of monovalent copper, 0.75 V to the mixed oxide (Cu(I)/Cu(II) oxide) region and 1.0 V to the stability region of divalent copper. After oxidation at E = 0.6 V for more than 1 h, two different reduction peaks are observed, suggesting the formation of two different layers in the film. These peaks are followed by a tail, presumably due to the reduction of copper ions present in the solution. The charge stored in the peak at higher potentials (0.3…0.35 V) is less influenced by the oxidation time than that stored in the peak at lower potentials (E < 0.2 V). This points to a bi-layer structure, in which only one of the layers grows appreciably in thickness with time. Numerical integration of the curve registered after 3 h of oxidation shows that the thickness of the part reduced at 0.3 V is ca. 3 times higher than that reduced at ca. 0.1 V. After oxidation at 0.75 V a third reduction peak appears at 0.6…0.65 V due to the formation of divalent Cu in the film.

An anodic excursion is observed during the negative-going potential sweep at 0.55…0.85 V after oxidation at 1.0 V, in accordance with the result shown in Fig. 3a. This is a strong indication of local damage of the oxide film, i.e. susceptibility to pitting of the material. It is worth noting that the amount of oxide reduced at 0.3...0.4 V is significantly smaller after oxidation at 1.0 V than at 0.6 V. This fact together with the fact that the ratio of the cathodic charge to the anodic charge is smaller points to the release of a higher amount of soluble products at 1.0 V.

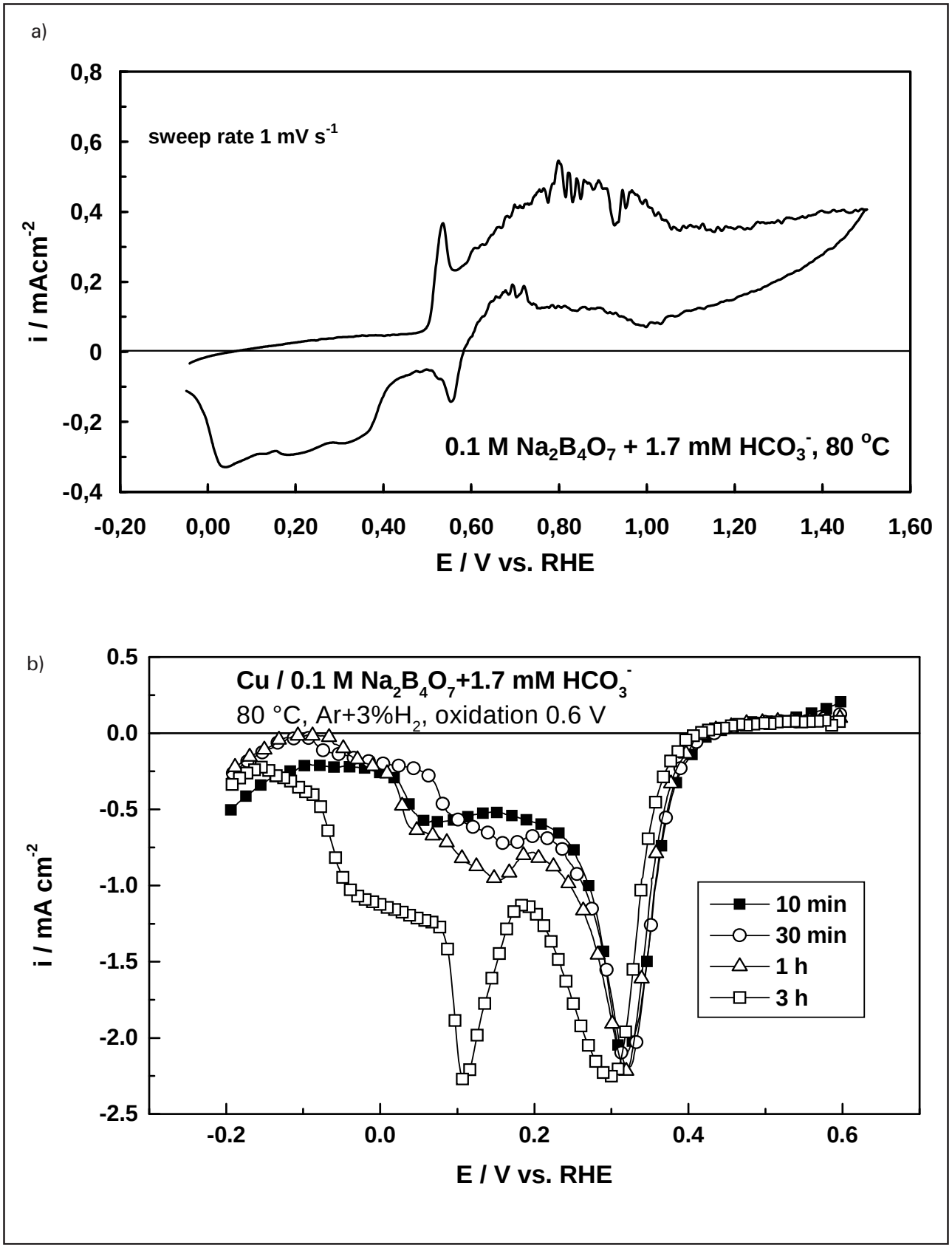

Fig 3. *Polarisation curve* ***a)*** *and negative-going potential sweeps after different oxidation times at* ***b)*** *+0.6 V for Cu OFP in 0.1 M $Na_2B_4O_7$ + 1.7 mM HCO_3^- at 80 °C and 2 MPa Ar+3% H_2. Sweep rate 1 mVs^{-1}.*

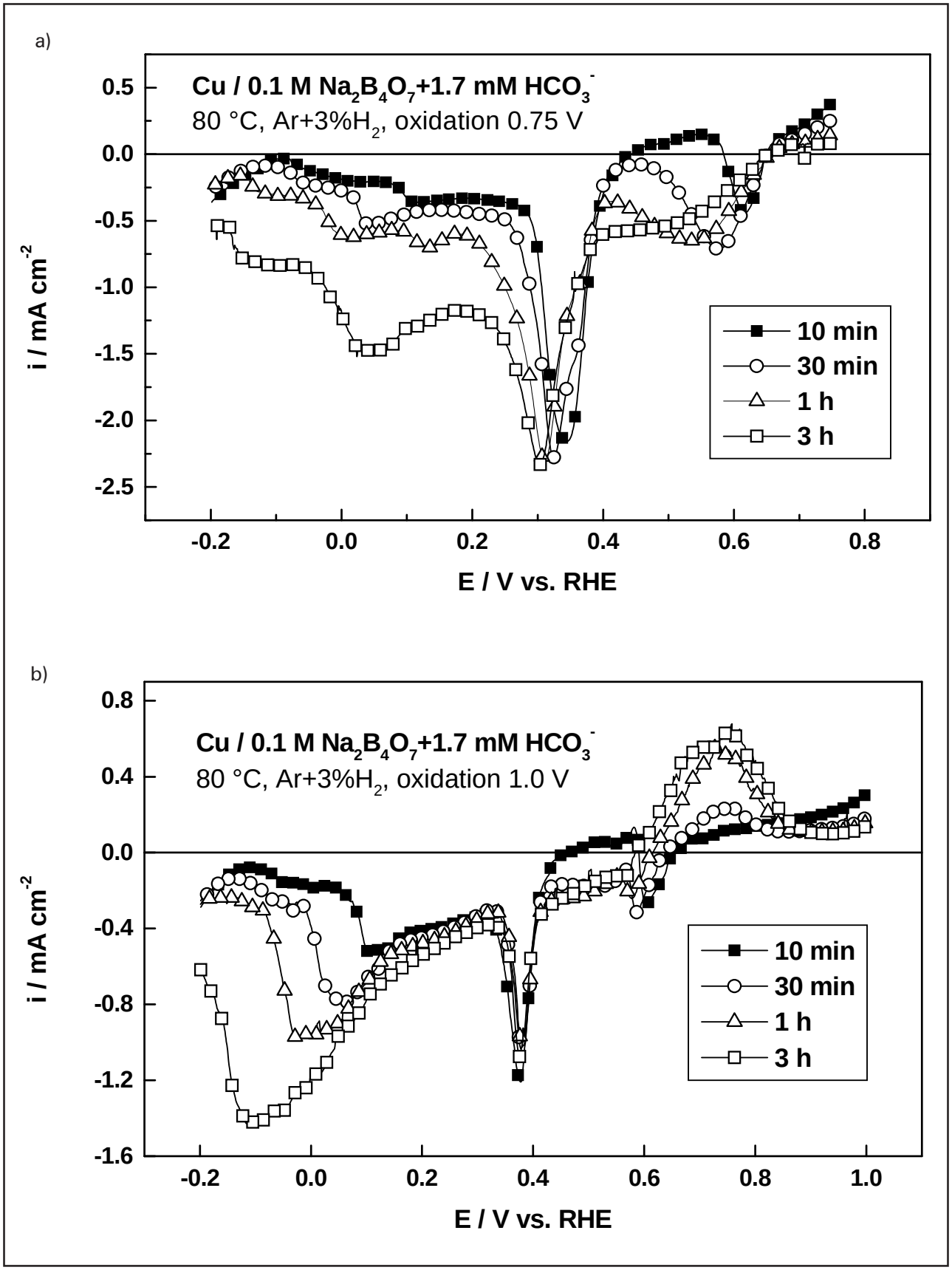

Fig 4. *Negative-going potential sweeps after different oxidation times at* ***a)*** *0.75 V and* ***b)*** *1.0 V for Cu OFP in 0.1 M $Na_2B_4O_7$ + 1.7 mM HCO_3^- at 80 °C and 2 MPa Ar+3% H_2. Sweep rate 1 mVs^{-1}.*

3.2.2 Electronic resistance of the oxide film formed on copper

The electronic resistance of the oxide film formed on Cu in 0.1 M $Na_2B_4O_7$ containing 1.7 mM HCO_3^- ions during a positive-going potential sweep is shown in Fig. 5a. It is in close agreement with the corresponding result in HCO_3^- -free 0.1 M $Na_2B_4O_7$ [10,11]. After the formation of a steady state film at E = 0.6 V, the resistance exhibits a value (see Fig. 5b) that is about ten-fold when compared to the corresponding value in pure 0.1 M $Na_2B_4O_7$ [10,11]. This might be due to the formation of a thicker or less defective semiconductor part of the layer in the stability region of monovalent copper in the presence of HCO_3^- ions. When the potential is cycled between 0.6 V and 0.9 V, the resistance at E = 0.9 V shows about the same values as in pure 0.1 M $Na_2B_4O_7$. This points to more profound changes in the structure of the film as a function of

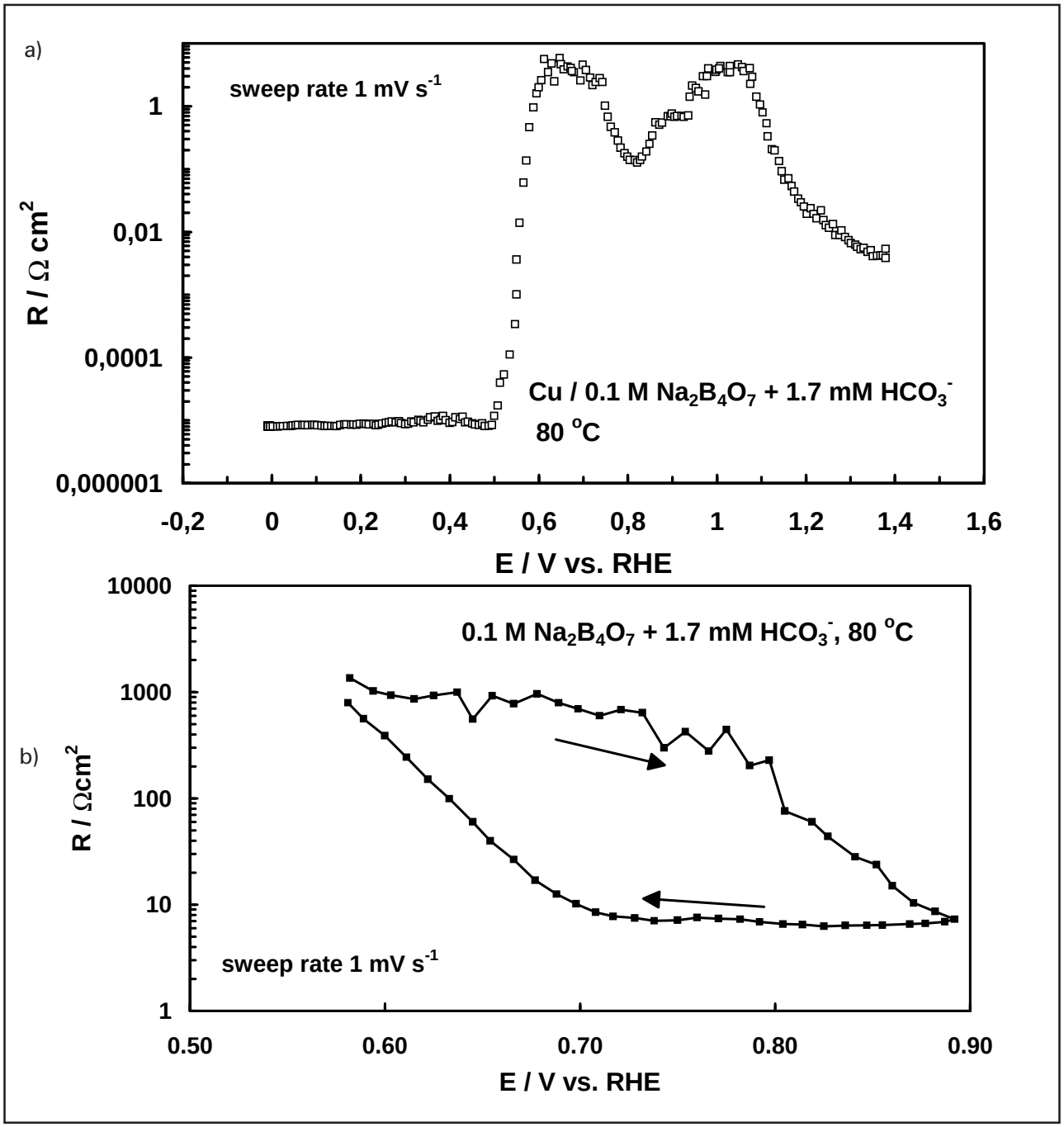

Fig. 5. *Electronic resistance* ***a)*** *of the film formed on Cu during a positive-going potential sweep and* ***b)*** *during a cyclic potential sweep after oxidation at 0.6 V for 0.5 h in 0.1 M $Na_2B_4O_7$ + 1.7 mM HCO_3^- at 80 °C and 2 MPa Ar+3% H_2.*

potential than in the case of pure 0.1 M $Na_2B_4O_7$. These changes may be connected with the formation of defects in the film or its partial destruction, which is in agreement with the anodic excursion in the i-E curve discussed above (Fig. 4b).

After oxidising Cu in the presence of HCO_3^- ions at 0.75 V and at 1.0 V and switching to open circuit, the electronic resistance first increases with decreasing potential (Fig. 6). However, the R-t curve following oxidation at 1.0 V shows a clear minimum when the potential has decayed to 0.6…0.7 V. This kind of minimum is very weak in the case of pure $Na_2B_4O_7$ [10], which again points to a more defective structure of the film in this potential region in the presence of HCO_3^- ions when compared to pure tetraborate.

3.2.3 Electrochemical impedance response of the oxide film formed on copper

Figures 7 a…c show the electrochemical impedance spectra of Cu oxidised at 0.6 V(a), 0.75 V (b) and 1.0 V (c) for 3…17 h. The results point to two dominating processes in the stability region of monovalent copper and in the mixed oxide (Cu(I)/Cu(II) oxide) region. The process resulting in the time constant at higher frequencies could be rela-

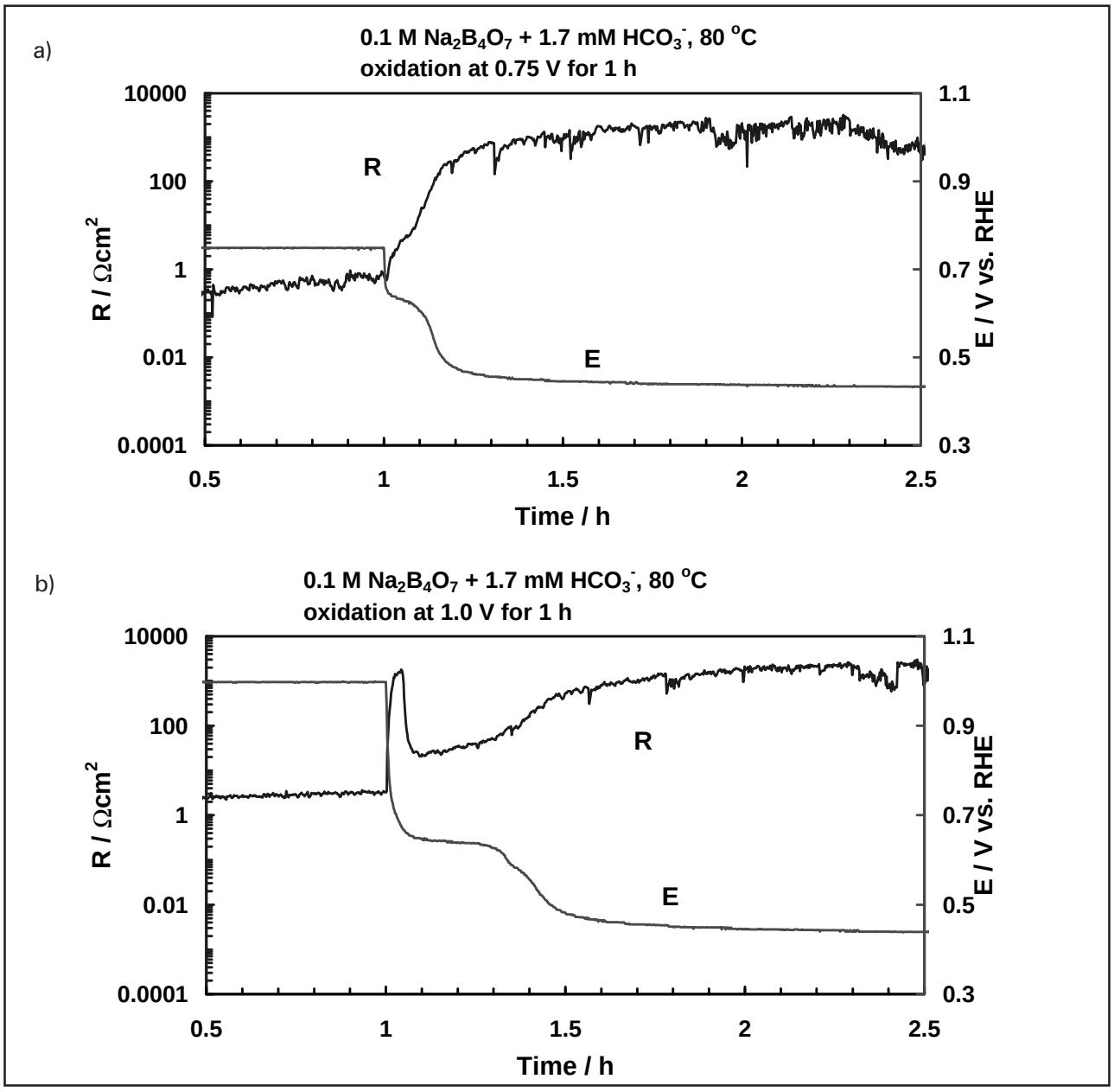

Fig. 6. *Open circuit potential decay curves and the corresponding resistance vs. time curves for Cu oxidised for 1 h at* ***a)*** *0.75 V and* ***b)*** *1.0 V in 0.1 M $Na_2B_4O_7$ + 1.7 mM HCO_3^- at 80 °C and 2 MPa Ar+3% H_2.*

ted to the electronic properties of the semiconductor part of the film, while that at lower frequencies is a transport process. For the film formed in the stability region of divalent copper, the contribution of the semiconductor part was no more discernible and some evidence for a transport process in a porous medium is seen.

The spectra shown in Figs 7 a...b (oxidation at 0.6 and 0.75 V, i.e. in the monovalent and the mixed oxide region) can be described with the following transfer function

$$Z = R_{el} + 1 / (1/R_t + j\omega C) + \sigma \tanh [(j\omega\tau_d)^{0.5}] / (j\omega)^{0.5}$$

where R_{el} is the electrolyte resistance, R_t and C are charge transfer resistance and high-frequency capacitance, respectively, σ is the Warburg constant and τ_d is the time constant of the transport process. As the transport process can be described by a finite-length Warburg impedance [12], it most probably occurs in the barrier part of the anodic film. At 1.0 V, the determination of the time constant of the transport process (τ_d) was impossible because of the unrealistically low measurement frequencies needed (Fig. 7c). That is why only the values of the Warburg constant (σ) were calculated for this potential. Furthermore, the exponent of the Warburg function at 1.0 V was found to be

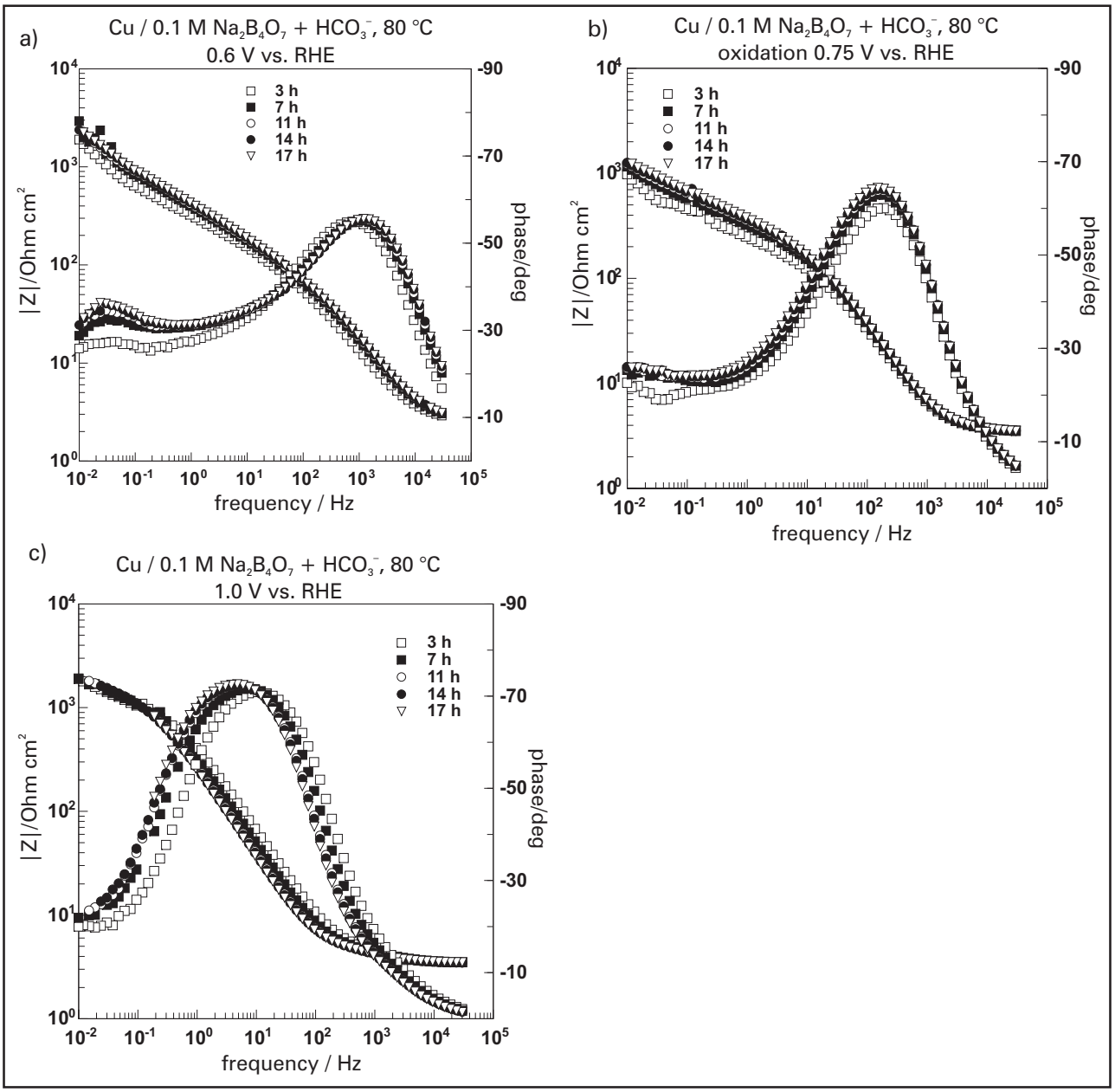

***Fig. 7**. Electrochemical impedance spectra of Cu oxidised at **a)** 0.6 V, **b)** 0.75 V and **c)** 1.0 V in 0.1 M $Na_2B_4O_7$ + 1.7 mM HCO_3^- at 80 °C and 2 MPa Ar+3% H_2 pressure for 3...17 h .*

Table I. *Best-fit values of the Warburg constant σ, the diffusion time constant τ_d, the charge transfer resistance R_t and the high-frequency capacitance C for Cu oxidised at 0.6, 0.7 and 1.0 V in 0.1 M $Na_2B_4O_7$ + 1.7 mM HCO_3^- for 3...17 h.*

	σ / Ω cm² $s^{-1/2}$			τ_d / s		R_t / Ω cm²			C / μFcm^{-2}		
t / h	0.6 V	0.75 V	1.0 V	0.6 V	0.75 V	0.6 V	0.75 V	1.0 V	0.6 V	0.75 V	1.0 V
3	511	232	500	37.7	79.8	70	60	720	6.2	11	81
7	739	272	320	51.1	129	66	80	1080	4.76	22	102
11	982	284	340	59.2	177	66	90	1100	4.62	20	100
14	1373	293	340	62.3	199	66	90	1120	4.55	21	102
17	1424	303	320	72.3	195	70	100	1100	4.45	20	105

considerably less than 0.5 implying e.g. transport in a porous medium [13]. The best-fit values of the parameters σ, τ_d, R_t and C are collected in Table I for all potentials.

The values of the charge transfer resistance practically do not change with time at 0.6 V, but increase up to 11 h oxidation at 0.75 V and 1.0 V. The capacitance values at 0.6 V decrease slowly with time and can by order of magnitude be associated with a thin space charge layer, whereas at 0.75 V the capacitance values practically do not change after 7 h of oxidation and are considerably greater, i.e. the space charge layer is much thinner or more defective. At 1.0 V, the capacitance values can be identified with those of a double layer, i.e. no evidence is found for a space charge layer. The Warburg constant increases continuously with time at 0.6 V probably indicating a decrease in the concentration and/or diffusion coefficient of the transported defects. This points to a certain stabilization process of the layer in the stability region of monovalent copper. The Warburg constant values are considerably lower and stay approximately constant both at 0.75 and 1.0 V implying a faster transport rate in the stability region of divalent copper. Thus the layer contains probably a higher concentration of defects in this region than in the region of monovalent copper.

The plots of C^{-2} vs E (i.e. Mott-Schottky plots) for films formed on Cu at 0.75 V and 1.0 V during oxidation for 1 and 16 h are shown in Fig. 8. In all the cases a linear portion in the curves can be recognised at E < 0.65 V, i.e. in the region where the film is composed mainly of monovalent copper. Any quantitative conclusions from the linear part are based on the assumptions that the defect concentration remains approximately constant over a narrow potential range and that the dielectric constant of the film does not change. The acceptor density decreases with time which is in line with the values of the Warburg constant collected in Table 1 for the potential of 0.6 V. What is more important, the acceptor density of the film in the monovalent region is higher in the case when the film was first formed at E = 1.0 V than at 0.75 V. This again points to the formation of a more defective film at positive potentials and hence to an increased susceptibility to localised corrosion.

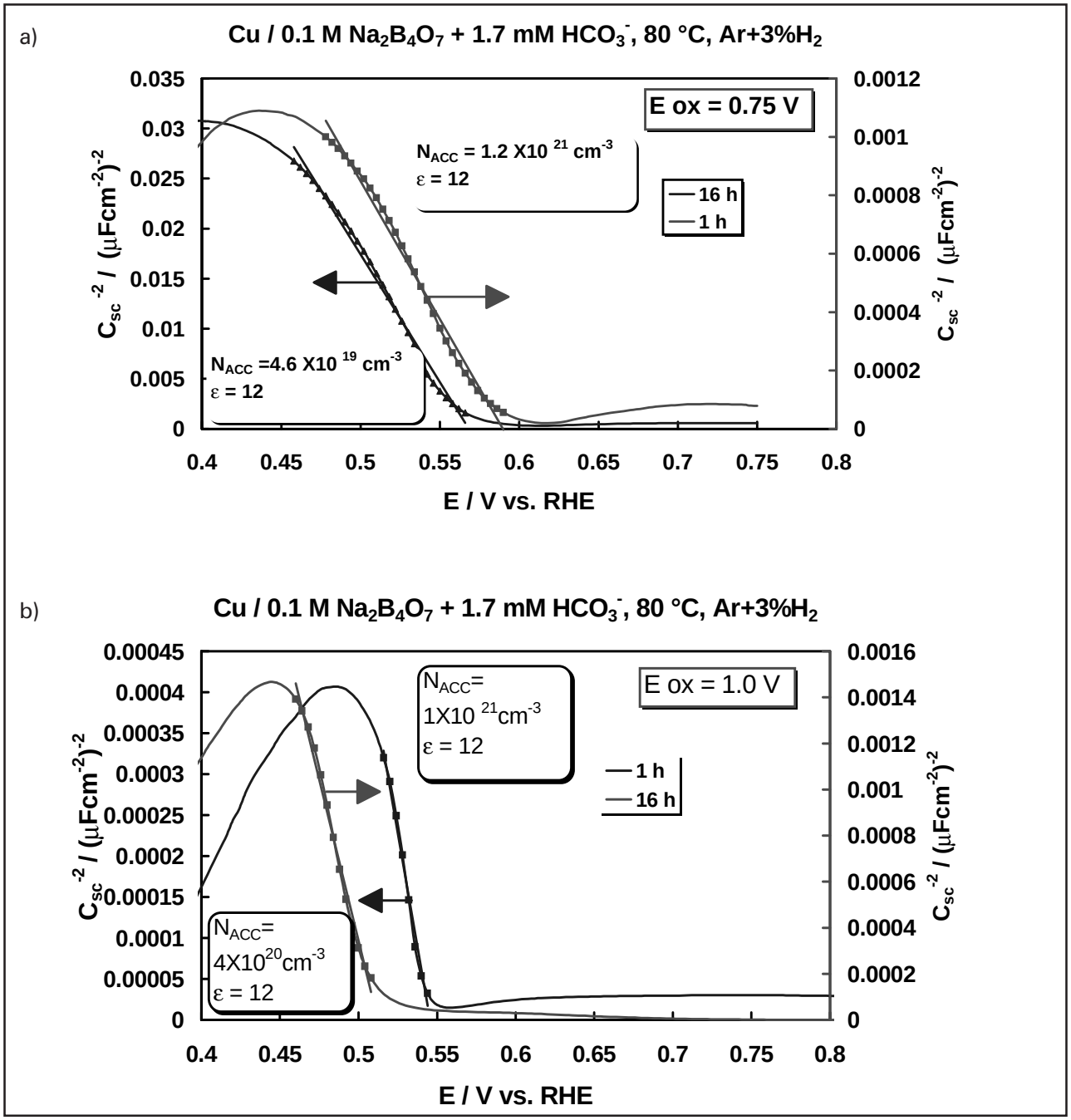

Fig. 8. *Mott-Schottky plots for films formed on Cu during oxidation at* ***a)*** *0.75 V and* ***b)*** *1.0 V in 0.1 M* $Na_2B_4O_7$ *+ 1.7 mM* HCO_3^- *at 80 °C for 1 and 16 h.*

4 CONCLUSIONS

The studies reported in the literature indicate that HCO_3^- ions increase the solubility of copper in the stability region of Cu(II). Thus they render the oxide film formed on copper susceptible to local damage and thus to localised corrosion at positive potentials. Unfortunately, environments in most of the studies reported in the literature are not comparable with repository conditions.

The results obtained in the experimental part of this work point to a bilayer structure of the anodic film on copper in neutral solutions containing bicarbonates. In the stability region of monovalent copper and in the mixed oxide (Cu(I)/Cu(II) oxide) region, the transport of ionic defects through a thin continuous p-type semiconductor layer is the rate limiting step of the anodic oxidation of copper. Anodic films formed in the stability region of divalent copper, do not show well-pronounced semiconductor behaviour. Substantial evidence was found in the voltammetric, CER and impedance results for the increased defectiveness of the anodic film in the divalent copper region. The anodic oxidation rate in the divalent copper region is presumably limited by interfacial charge transfer and transport of ions through the very defective and/or porous anodic layer. Thus bicarbonates render the Cu/anodic film system more susceptible to metastable pitting and related localized corrosion phenomena at positive potentials. High positive potential may however not be relevant in repository conditions. Accordingly, it can be suggested that bicarbonate ions alone are not likely to pose a serious hazard to the stability of copper oxide films on the shield of the canister.

5 SUMMARY

Copper is used as an outer shield of cast iron canisters planned for storage of spent nuclear fuel. The copper shield is responsible for the corrosion protection of the canister. The aim of the present work was to study and discuss the influence of bicarbonate (HCO_3^-) anions on the stability of the copper oxide film. The work consists of a brief literature survey and an experimental part, in which voltammetry, electrochemical impedance spectroscopy and dc resistance measurements via the contact electric resistance (CER) technique were used as the main techniques.

The studies reported in the literature indicated that HCO_3^- ions increase the solubility of copper in the stability region of Cu(II). Thus they render the oxide film formed on copper susceptible to local damage and to localised corrosion at positive potentials. Unfortunately, despite the great importance of bicarbonates in copper corrosion, most of the environments used in the electrochemical and corrosion studies are not comparable with repository conditions. In the existing studies either the bicarbonate concentrations or pH of the solutions were too high. In addition, no such studies were available, in which not only the effect of carbonate ions, but also possible synergetic effects of these species with other aggressive ions would have been clarified.

The voltammetric results obtained in the experimental part of this work point to a bilayer structure of the anodic film on copper in neutral solutions containing bicarbonate ions. The transport of ionic defects through a thin continuous p-type semiconductor layer was concluded to be the rate limiting step of the anodic oxidation of copper in the stability region of monovalent copper and in the mixed oxide (Cu(I)/Cu(II) oxide) region. Films formed in the divalent copper region did not show well-pronounced semiconductor behaviour. Substantial evidence was found in the voltammetric, CER and impedance results for the increased defectiveness of the anodic film in the divalent copper region. The oxidation rate of copper in the divalent region was suggested to be limited by interfacial charge transfer and transport of ions through the very defective and/or porous anodic layer.

The present experimental results strongly indicate that bicarbonate ions render the Cu/anodic film system more susceptible to metastable pitting and related localized corrosion phenomena at positive potentials. High positive potential may however not be relevant in repository conditions. Accordingly, it can be suggested that bicarbonate ions alone are not likely to pose a serious hazard to the stability of copper oxide films on the shield of the canister.

REFERENCES

1 Sanchez, Perez M.; Barrera, M.; Gonzalez, S.; Souto, R. M.; Salvarezza, R. C.; Arvia, A. J., Electrochemical behaviour of copper in aqueous moderate alkaline media, containing sodium carbonate and bicarbonate, and sodium perchlorate, Electrochimica Acta Vol.35, No. 9, 1990, p 1337–1343.

2 M. Drogowska, L. Brossard, H. Menard, Effect of temperature on copper dissolution in NaHCO//3 and NaHCO//3 plus NaCl aqueous solutions at pH 8, Journal of the Electrochemical Society Vol.140, No.5, 1993, p 1247–1251.

3 Ribotta S.B., Folquer M.E. and Vilche J.R., Influence of bicarbonate ions on the stability of prepassive layers formed on copper in carbonate-bicarbonate buffers, Corrosion Science, Vol.51, No .9, 1995, p 682–688.

4 Drogowska, M.; Brossard, L.; Menard, H., Comparative study of copper behaviour in bicarbonate and phosphate aqueous solutions and effect of chloride ions, Journal of Applied Electrochemistry Vol.24, 1994, p 344–349.

5 Gassa L.M., Ribotta S.B., Folquer M.E. and Vilche J.R., Influence of temperature on dissolution and passivation of copper in carbonate-bicarbonate buffers, Corrosion, Vol.54, No. 3, 1998, p179–186.

6 Thomas, J.G.N.; Tiller, A.K., Formation and Breakdown of Surface Films on Copper in Sodium Hydrogen Carbonate and Sodium Chloride Solutions. I. Effects of anion concentrations, British Corrosion Journal Vol.7, 1972, p 256–262.

7 Thomas, J.G.N.; Tiller, A.K., Formation and Breakdown of Surface Films on Copper in Sodium Hydrogen Carbonate and Sodium Chloride Solutions. I. Effects of temperature and pH, British Corrosion Journal Vol.7, 1972, p 263–267.

8 Alhajji, J.N.; Reda, M.R., Role of solution chemistry on corrosion of copper in synthetic solutions: Effect of bicarbonate ion concentration on uniform and localized attack, British Corrosion Journal Vol.31, No.2, 1996, p 125–131.

9 M. Bojinov, J. Hilden, T. Laitinen, J. Piippo, T. Saario, in *Proceedings of EUROCORR'98*, The European Corrosion Congress, p.73, Utrecht, The Netherlands, (1998).

10 J. Piippo, T. Saario, T. Laitinen, M. Bojinov, J. Hinttala, *Materials Sci. Forum*, 289–292, 429 (1998).

11 J. Piippo, T. Saario, T. Laitinen, M. Bojinov, J. Hilden, J. Hinttala, in *Passivity and Its Breakdown /1997*, P. Natishan, H. Isaacs, M. Janik-Czachor, V. Macagno, P. Marcus and M. Seo, Editors, PV 97-26, p.925, The Electrochemical Society Proceedings Series, Pennington, NJ (1998).

12 J.R. Macdonald and D.R. Franceschetti, in *Impedance spectroscopy, Emphasizing Solid Materials and Systems*, J.R. Macdonald, Editor, p. 88, John Wiley & Sons, New York (1987).

13 C. Gabrielli, *Identification of Electrochemical Processes by Frequency Response Analysis*, Tech. Rep. No. 004/83, p. 50, Solartron Instruments, Farnborough, England, (1984).

PART II: BOUNDARY CONDITIONS

Generally, the groundwater flow conditions evolve with time, and the changes (e.g. due to glaciations) affect especially the boundary conditions of the problem. However, the emphasis in this study is on the steady-state conditions of the present day. In chapter 10, the flow field is calculated for a situation of static, conceptual boundary conditions in a 2-dimensional regional scale in a vertical position.

8 PHYSICAL BACKGROUND

This section discusses the boundary conditions encountered in saturated groundwater flow, i.e. in which the whole flow system is full of water. The approach is for a steady state, where the flow is independent of time. In the approach, we will consider the boundary conditions in mathematical sense and how they are related to the physical conditions in saturated groundwater flow systems. The special role of the water table as a boundary is reviewed separately.

8.1 Classifications

The classification of the boundary conditions is based on the knowledge of the behaviour of physical quantities (e.g. potential and flux) on a boundary. Mathematically, the three basic situations are the following [15].

1. *Dirichlet condition* of a prescribed potential, where the potential on a boundary is a known function of position (and time): $h(x,y,z,t) = f(x,y,z,t)$.

2. *Neumann condition* of a prescribed flux, where the normal derivative of the potential on a boundary is a known function of position (and time): $\partial h(x,y,z,t)/\partial n = f(x,y,z,t)$.

3. *Mixed condition*, which is a combination of the Dirichlet and Neumann conditions on a boundary: $a(x,y,z,t)\cdot h(x,y,z,t) + b(x,y,z,t)\cdot(\partial h(x,y,z,t)/\partial n) = f(x,y,z,t)$.

The mixed condition is the most general one, from which the other two conditions can be reduced. Furthermore, additional and commonly used types of boundary conditions can be reduced from the Dirichlet and Neumann conditions, when the known functions of position and time are constants (or zero). In addition, two extra types of boundaries are encountered in groundwater flow.

Consequently, seven principal types of boundary conditions in saturated groundwater systems are defined [16, 11].

1. *Prescribed head boundary (Dirichlet condition)*: A specified potential boundary is encountered when an aquifer is in direct hydraulic contact with a river or a lake in which the water level is known. The head in the bounding body of water changes in relation to the slope of its water surface. Thus, the boundary condition depends on the condition of a region outside of the modelling domain and is supposed to be unaffected by the possible changes in the modelling domain (e.g. excavational disturbances).

2. *Constant head boundary (constant Dirichlet condition)*: This type of boundary is a special case of the Dirichlet condition defined above, where an aquifer is bounded by an essentially stationary body of water (e.g. a lake), in which the head does not vary.

3. *Prescribed flux boundary (Neumann condition)*: In this case the flow across the boundary is a known function of position (and time). A special case of this is a constant-flux boundary on which the crossing flow has a regionally constant rate.

4. *Streamline (stream surface) boundary (zero Neumann condition)*: This is the *no-flow condition*, which is commonly used in the context of the safety analysis of nuclear waste disposal. Stream surfaces are perpendicular to the equipotential surfaces (surfaces of constant head) and tangent to the flow velocity vectors and, consequently, flow does not cross a stream

surface. An effectively impermeable wall, like the contact between sand and solid rock is an example of a boundary of this type.

5. *Head-dependent flux boundary (mixed condition)*: In this case, flux across a boundary surface changes in response to changes in head within the water system adjacent to the boundary. An example of this type is a semipervious boundary consisting of clay.

6. *Free surface boundary*: The most common free surface boundary is a water table, which is the boundary surface between the saturated flow field and the atmosphere. The pressure at the water table is atmospheric and the pressure head equals zero. Thus, the total groundwater head at points along the water table is just equal to the elevation head, or $h = z$. This situation is analogous to the head at the surface of a static fluid body. Another example of a free-surface boundary is the transition between fresh and saline water in a coastal aquifer. If we neglect diffusion and assume the saline groundwater seaward of the interface to be stationary, the freshwater-saltwater transition zone can be treated as a sharp interface and can be taken as the bounding stream surface (a *no-flow boundary*) of the fresh groundwater flow system. Under these conditions, the freshwater head at points on the interface (or within the saltwater body) varies only with the elevation, z, and the freshwater head at any point on this idealised stream-surface boundary is thus a linear function of the elevation of that point.

7. *Seepage surface boundary*: This is a boundary between a saturated flow field and the atmosphere, along which groundwater discharges, either by evaporation or due to gravity. Free surface is a special case of this, in which there is no discharge. The equation for the seepage surface condition is the same that for a free surface, $h = z$. Seepage face is neither an equipotential line nor a streamline. Seepage faces are often neglected in models of large aquifer systems because their effect is often insignificant at the regional scale of problem definition.

The last two boundary types—free surface and seepage surface—are unique to liquid-flow systems governed by the gravity force and have no counterpart in systems involving heat flow or flow of electrical current.

8.2 The water table as a boundary

In the Finnish approach to groundwater flow modelling in the analysis of nuclear waste disposal, the boundary conditions at the vertical sides as well as on the bottom of the model are typically assigned to be no-flow conditions. The selection of the condition on the top boundary, i.e. on the water table, is then a crucial factor for the solutions, especially in the simplified cases. The various ways of treating the water table as a boundary are the following [16].

1. It is usually conceptualised as a free surface recharge boundary—either where recharge equals zero and the water table is a stream surface or where recharge equals a specified value.

2. As a discharge boundary, particularly where it is near land surface and thus is subject to losses by evaporation and transpiration. The discharge from the water table in this case is conceptualised as a function of the water table elevation and the water table as a head-dependent flux boundary.

3. When the position of the water table is fixed as part of the problem definition, it can be treated as a prescribed head boundary.

9 BOUNDARY CONDITIONS IN THE SAFETY STUDIES

The approaches to define boundary conditions differ considerably in the reports of Sweden and Finland. While the Finnish studies use essentially the assumption of the existence of no-flow boundaries, the Swedish studies consider the situation more complicated.

9.1 The Finnish approach

In the Finnish studies, the approaches to define the boundary conditions are consistent [4, 3, 7, 10]. The modelling area is assumed to begin from under the highly conductive surface layer of ground and fractured rock. Near the ground surface, flow is nearly parallel to the ground surface and the hydraulic head of the elevation of the water table is transferred lower as such and used as the boundary condition for the top surface of a model.

The groundwater flow is assumed to decrease with depth and the bottoms of various models (with varying depth of the bottom boundary at various sites) are defined as no-flow boundaries.

The sides of the modelling areas are extended outside the borders of the investigation areas to supposed no-flow boundaries. This condition is assumed to prevail on boundaries associated with

- main water divides,
- surfaces parallel to the assumed direction of the groundwater flow,
- rivers and lakes,
- sea and
- regional fracture zones lying far from the investigation areas.

The bounding faces of the flow model are thus assumed to be closed for the flow also deep in the bedrock. The sides bounded by sea are considered no-flow boundaries because flow through the interface of fresh and saline water is negligible. This condition forces the groundwater flowing towards the sea to rise on the ground.

The prescription of the groundwater flux on a boundary would require that

- the hydraulic conductivity and
- the gradient of the hydraulic head

should be known. In practice, this seems to be impossible. The sides of the models are expanded to supposed no-flow boundaries, because, in practice, reliable boundary conditions can be achieved only on boundaries through which ground water does not flow. The boundaries should also be far enough from the investigation areas to make the significance of the uncertainties associated with the boundaries small.

The no-flow side boundaries are used for the regional scale calculations. For smaller scale, the boundary conditions are the hydraulic heads calculated with the regional model.

9.2 The Swedish approach

In the Swedish studies, the DF and SC models are used for site scale modelling. However, they have (especially DF) dimensions and boundary conditions comparable with those in the Finnish regional scale studies. The regional model of the Swedish approach is simply a reproduction of the groundwater flow field driven by the elevation of the water table. The boundary conditions for smaller scales (semiregional/site scale) are at least conditioned by the results for the regional scale modelling. The approach is as applied to the Äspö site [1, 2].

9.2.1 The DF site model

For the base case, the conditions at the upper boundary are specified as uniform infiltration on land, and fixed heads equal to the water surface elevation are specified at points undersea and under a freshwater lake. For a variant case, the on-land portion of the upper boundary is assigned fixed heads equal to the topographic elevation.

For the base case, the condition at the bottom of the model is no-flow. For variant cases, fixed, declining heads at the bottom such as could effectively be produced by a highly transmissive, subhorizontal, regional fracture zone just below the bottom of the model, are applied.

For the base case, a fixed head is assigned on the landward and no-flow condition on the seaward vertical boundaries of the semiregional domain. For variant cases, fixed heads are assigned on the seaward boundary [1].

9.2.2 The SC site model

The SC model domain is relatively small and idealised and, consequently, the boundary conditions are also simplified. A prescribed hydraulic head is assigned on the top boundary as well as on the bottom boundary, which in the SC model is positioned at the depth of a repository. The sides of the model are vertical no-flow boundaries.

The hydraulic head difference between the top and bottom boundaries is rescaled to give a fixed, effective hydraulic head gradient, which corresponds to a typical head gradient calculated with the DF model. This configuration of boundary conditions implies that the flow is always directed upwards in the SC model [2].

10 BOUNDARY CONDITIONS IN A REGIONAL MODEL FOR EC APPROACH

The dimensions of the regional models for the Finnish sites vary. The geometry for the regional model of the Olkiluoto site is used as an example in this study, but the boundary conditions are fictitious to study the conceptual dependence of the solution on different boundary conditions. The approach is simplified utilising the EC model without fractures in a 2-dimensional vertical cross-section.

10.1 Geometry of the modelling domain

According to [9], the largest length of the regional modelling domain covering the whole Olkiluoto island is approximately 6.3 km and the depth of the domain is chosen to be 1500 m. The size of the repository in this study is chosen to be L = 700 m, on account of the figures in [8, p. 41].

In this study, the Matlab® PDE-toolbox is used with a vertical 6300×1500 m modelling domain, in which $x \in [-3150, 3150]$ m and $y \in [-1500, 0]$ m. The calculations are performed for both the natural state and the state with a repository, in which the repository is represented by a vertical 700×10 m plate at the depth of 500 m.

In the base case

- the sides and the bottom of the model are assigned a no-flow condition and
- the boundary condition on the top surface of the model is given fictitious values.

A sensitivity analysis comprises cases, in which

- the side boundaries are expanded farther or
- a prescribed head is assigned at the bottom of the domain.

10.2 The equations and parameters

The task is to calculate the stationary head and flow fields, without sources or sinks present in the domain and with a constant density of the ground water, i.e. the heads with the aid of (31)

$$\nabla \cdot (\mathbf{K} \nabla h) = 0, \tag{31}$$

and the Darcian velocities from (5)

$$\mathbf{q} = -\mathbf{K} \nabla h. \tag{5}$$

The hydraulic conductivity of the intact rock in Olkiluoto varies exponentially with depth as

$$K(y) = K_0 \cdot 10^{-ry}, \tag{36}$$

where K_0 is the hydraulic conductivity on the surface, y(m) is the depth and r is the depth-dependence coefficient. The numerical values derived for the Olkiluoto site in [9] are

$K_0 = 1.78 \cdot 10^{-9}$ m/s,

$r = 4.98 \cdot 10^{-3}$ 1/m.

In the base case, the no-flow condition is assumed to prevail at the bottom and on the sides of the model. Thus, in the natural state the factors affecting the solution are the variation of the top boundary condition and the variation of the conductivity of rock.

As stated in chapter 4.1, the elevation of the water table varies in Finland essentially with the topography of the ground surface. Thus, as in the Finnish studies (chapter 9.1), the elevation of the water table or, alternatively, the elevation of the ground surface is here used as the top boundary condition.

The additional parameter for the state with a repository is the conductivity of the repository, K_{Rep}, which can be considerably larger or smaller than that of the surrounding rock. The maximum value of K on the ground surface is $K_0 = 1.78 \cdot 10^{-9}$ m/s and the value at the depth of a repository (500 m) from (36) is

$K_{500} = 5.76 \cdot 10^{-12}$ m/s,
so at the depth of 500 m K is less than 1/300 of that near the ground surface.

In this study, the conductivity of the repository plate is chosen to vary in the range of 1/100–100 times the conductivity of the surrounding rock, K_{500}. The results for the state with a repository are calculated for 4 different cases:

1. $K_{Rep} = 1/100 \cdot K_{500}$,
2. $K_{Rep} = 1/10 \cdot K_{500}$,
3. $K_{Rep} = 10 \cdot K_{500}$,
4. $K_{Rep} = 100 \cdot K_{500}$.

10.3 Variation of the top boundary condition

10.3.1 Variation at the Finnish sites

Most of the regional domain of Olkiluoto is occupied by the Olkiluoto island [9], on which the elevation of the water table varies as $z \in [0,10]$ m. The largest values are found at the central parts of the island, where the proposed repository is located and the smallest values on the shore.

In Kivetty, the regional variation of the annual average of the water table elevation is approximately $z \in [100, 200]$ m. The topography is more undulating than in Olkiluoto. However, the largest values occur near the centre and the smallest near the sides of the regional domain [7].

The regional variation of the topography is the largest at the Romuvaara site. The elevation of the water table in the site model varies as $z \in [190, 222.5]$ m. At the boundaries of the regional model, there exist values in the range $z \in [175, 260]$ m. The proposed repository is located under a large hill [17].

10.3.2 Fictitious variation

The conceptual, fictitious top boundary conditions used in this study are of the prescribed head type, which resemble the topography of the domain. The fictitious variation is assumed to be within realistic range according to the information on the actual variation (section 10.3.1).

The chosen cases for the head on the top boundary are the following:

- A linearly varying head resembles the hill of a constant slope across the domain. Two variants are employed, the ranges of which are
  - in the base case $h \in [0, 10]$ m ($h = 5 + x/630$ m) and
  - in the variant case $h \in [0, 100]$ m ($h = 50 + x/63$ m).
- A parabolic head resembles a hill, the peak of which is located in the centre of the domain. Two variants are employed, the ranges of which are
  - in the base case $h \in [0, 10]$ m ($h = -x^2/992250 + 10$ m) and
  - in the variant case $h \in [0, 100]$ m ($h = -x^2/99225 + 100$ m).
- A cosine-shaped head resembles an undulating topography with consecutive hills and valleys. Three variants are employed.
  - In the base case $h \in [0, 10]$ m ($h = 5 \cdot \cos(3\pi \cdot x/3150) + 5$ m) and land inclines (declines) at most 10 m by every 1050 m
  - In the first variant case $h \in [0, 100]$ m ($h = 50 \cdot \cos(3\pi \cdot x/3150) + 50$ m) and land inclines (declines) at most 100 m by every 1050 m.
  - In the second variant case $h \in [0, 10]$ m ($h = 5 \cdot \cos(15\pi \cdot x/3150) + 5$ m) and land inclines (declines) at most 10 m by every 210 m.

The different top boundary conditions are illustrated in Figure 1.

10.4 The results

The results for the head and flow fields in the whole modelling domain for the natural state are illustrated in the appendices 1–4 and for the state with a repository in Appendices 5–20. The contour lines represent lines of equal head, h(m) = constant. The orientation of the arrows indicate the flow direction and the length of each arrow is proportional to the absolute value of the Darcian velocity, q(m/s) = $|\mathbf{q}|$. It should be observed, that Darcian velocity is a measure of volume flux ($m^3/(m^2 s)$) and not of the velocity of the fluid.

For the state with a repository, the additional results of the variation of the flow pattern in the vicinity of the repository against the 4 chosen values of K_{Rep} are illustrated in Appendices 21–24,

in which the arrows are of equal length, i.e. not proportional to q.

In the following, the results for different cases are compared quantitatively by investigating

- q near the ground surface above the repository segment,
- the depth, at which q has dropped to 10 % of that near the ground surface and
- the range of q on the repository segment

in all the cases. Here, "repository segment" refers to the horizontal axis of the proposed location of a repository plate, i.e. the segment between the points $(x, y) = (-350, -500)$ m and $(x, y) = (350, -500)$ m. In addition, for the case with a repository, the variation of q in rock near the repository at the depth of 500 m against increasing K_{Rep} is studied.

The qualitative result obtained is the flow pattern in the whole domain and especially in the vicinity of the repository segment. Because of the relatively small values of q at the repository depth, the corresponding arrows are so short that the flow pattern is not visible in the vicinity of the repository segment in Appendices 1–20. The results for those patterns presented in the following sections as well as the quantitative results are based on a more detailed analysis of the solutions for the Darcian velocity fields, the images of which are not presented here. However, the flow around a repository for the state with a repository is illustrated in Appendices 21–24 for most of the cases.

The meshes used in the calculations for both the natural state (2993 nodes and 5760 triangles) and the state with a repository (9771 nodes and 19248 triangles) are presented in Appendix 27.

10.4.1 The natural state

Linear head

The flow in the whole domain is essentially horizontal from right to left with the largest values occurring near the ground surface.

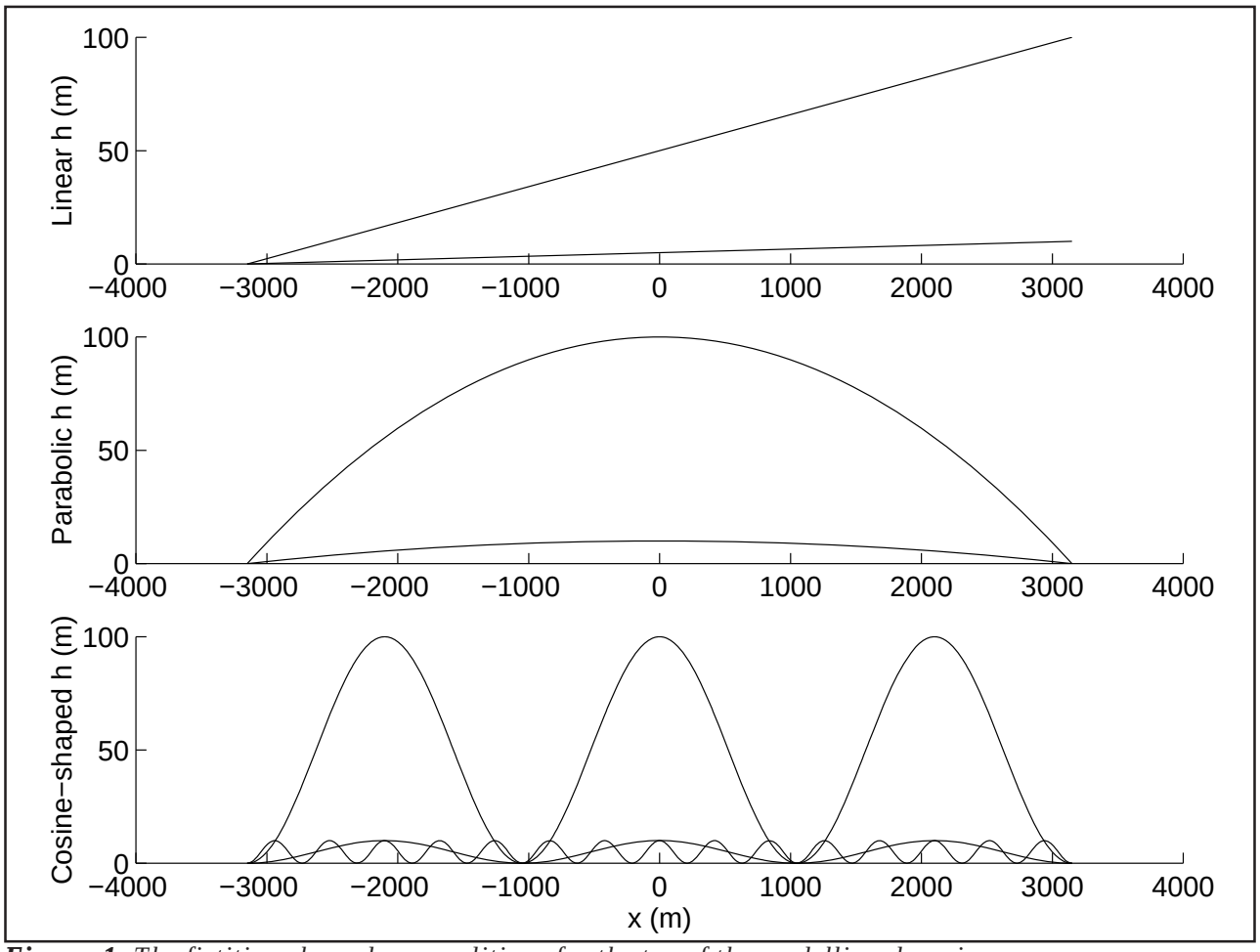

Figure 1. *The fictitious boundary conditions for the top of the modelling domain.*

The base case (App. 1):

The Darcian velocity, $q = 0.1 \cdot 10^{-13}$ m/s, is essentially constant on the whole repository segment. The largest values near the ground surface are $q = 0.2 \cdot 10^{-11}$ m/s and the value above the segment has dropped to 10 % of this approximately at the depth of 230 m.

The variant case:

The pattern of the result is not changed, only the scale is increased by a decade.

Parabolic head

The flow is from the centre of the ground surface to the sides of the model with the largest values of the Darcian velocity ($q = 0.9 \cdot 10^{-11}$ m/s in the base case) occurring near the upper corners of the domain.

The base case (App. 2):

On the centre of the repository segment, the direction of the flow is straightly downwards through the centre. On the sides of the segment, the flow is directed from above the repository to the left hand side of the segment under the repository on the left and to the right hand side under the repository on the right.

The range of the values of Darcian velocity on the repository segment is $q \in [0.1, 0.5] \cdot 10^{-14}$ m/s with the largest values occurring in the edges and the smallest in the centre of the segment. Near the ground surface above the repository segment, the Darcian velocity is $q = 0.2 \cdot 10^{-12}$ m/s and drops to 10 % of this approximately at the depth of 240 m.

The variant case:

The pattern of the result is not changed, only the scale is increased by a decade.

Cosine-shaped head

The flow is from under hills to under valleys and concentrates to the vicinity of the ground surface. The largest values of the Darcian velocity ($q = 0.2 \cdot 10^{-10}$ m/s in the base case) occur near the ground surface in the middle regions of the hills and valleys, where the flow is horizontal.

The base case (App. 3):

On the centre of the repository segment, the direction of the flow is straightly downwards through the centre. On the sides of the segment, the flow is directed from above the repository to the left hand side of the segment under the repository on the left and to the right hand side under the repository on the right.

The range of the values of Darcian velocity on the repository segment is $q \in [0.2, 0.5] \cdot 10^{-13}$ m/s with the largest values occurring in the edges and the smallest in the centre of the segment. Near the ground surface above the repository segment, the Darcian velocity is $q = 0.5 \cdot 10^{-11}$ m/s and drops to 10 % of this approximately at the depth of 220 m.

The first variant case:

The pattern of the result is not changed, only the scale is increased by a decade.

The second variant case (App. 4):

The variation of the result is more frequent than in the base case but still symmetrical and the flow pattern is more concentrated to the vicinity of the ground surface. On the centre of the repository segment, the direction of the flow is still straightly downwards, but on the sides of the segment, the flow is directed from above the repository through the centre of it.

The largest value of Darcian velocity occurring in various places near the ground surface is $q = 0.8 \cdot 10^{-10}$ m/s. The range of the values on the repository segment is $q \in [0.2, 0.4] \cdot 10^{-14}$ m/s with the largest values occurring in the centre and the smallest in the edges of the segment. Near the ground surface above the repository segment, the Darcian velocity is $q = 0.6 \cdot 10^{-10}$ m/s and drops to 10 % of this approximately at the depth of 150 m.

10.4.2 The state with a repository

Linear head

In every case, the flow in the whole domain remains essentially horizontal from right to left with the largest values occurring near the ground surface.

The base case (App. 5–8, 21):

As K_{Rep} increases from $1/100 \cdot K_{500}$ to $100 \cdot K_{500}$:

- The value of the Darcian velocity near the ground surface above the repository (q = $0.2 \cdot 10^{-11}$ m/s) and the depth (230 m) at which it is dropped to 10 % of this remain unchanged.
- The almost horizontal flow is gradually bent to go through the repository in the close vicinity of it. When the repository is non-conducting ($K_{Rep} = 1/100 \cdot K_{500}$), the flow is slightly curled around the repository. Meanwhile, the flow is clearly seen to go through the repository, when $K_{Rep} = 100 \cdot K_{500}$ (App. 21).
- The range of the Darcian velocity values on the horizontal axis of the repository plate increases gradually from $q \in [0.09, 0.1] \cdot 10^{-15}$ m/s, when $K_{Rep} = 1/100 \cdot K_{500}$ and the largest values occur on the edges of the repository, to $q \in [0.09, 0.6] \cdot 10^{-12}$ m/s, when $K_{Rep} = 100 \cdot K_{500}$ and the largest values occur in the centre of the repository.
- The Darcian velocities in rock near the repository at the depth of 500 m are slightly (less than one decade) increased.

The variant case:

The pattern of the result is unchanged, only the scale is increased by one decade.

Parabolic head

In every case, the flow remains essentially from the centre of the ground surface to the upper corners of the modelling domain.

The base case (App. 9–12, 22):

As K_{Rep} increases from $1/100 \cdot K_{500}$ to $100 \cdot K_{500}$:

- The value of the Darcian velocity near the ground surface above the repository (q = $0.2 \cdot 10^{-12}$ m/s) and the depth (240 m) at which it is dropped to 10 % of this remain unchanged.
- The flow pattern in the close vicinity of the repository is almost unchanged with the small values of K_{Rep}. When $K_{Rep} = 100 \cdot K_{500}$, more flow can be seen to go through the repository and after gone through, the flow is more straightly directed to the ground surface (App. 22).
- The range of the Darcian velocity values on the horizontal axis of the repository plate increases gradually from $q \in [0.2, 0.6] \cdot 10^{-15}$ m/s, when $K_{Rep} = 1/100 \cdot K_{500}$ to $q \in [0.09, 0.3] \cdot 10^{-13}$ m/s, when $K_{Rep} = 100 \cdot K_{500}$.
- The Darcian velocities in rock near the repository at the depth of 500 m are slightly (less than one decade) increased.

The variant case:

The pattern of the result is unchanged, only the scale is increased by one decade.

Cosine-shaped head

In every case, the flow remains essentially from under hills to under valleys and concentrates to the vicinity of the ground surface.

The base case (App. 13–16, 23):

As K_{Rep} increases from $1/100 \cdot K_{500}$ to $100 \cdot K_{500}$:

- The value of the Darcian velocity near the ground surface above the repository (q = $0.5 \cdot 10^{-11}$ m/s) and the depth (210 m) at which it is dropped to 10 % of this remain unchanged.
- When $K_{Rep} = 1/100 \cdot K_{500}$, the flow pattern in the vicinity of the repository is the same as in the natural case. When $K_{Rep} = 100 \cdot K_{500}$, the amount of flow through the edges of the repository is increased and after gone through, the flow is more straightly directed to the ground surface (App. 23).
- The range of the Darcian velocity values on the horizontal axis of the repository plate increases gradually from $q \in [0.3, 0.8] \cdot 10^{-14}$ m/s, when $K_{Rep} = 1/100 \cdot K_{500}$ to $q \in [0.07, 0.6] \cdot 10^{-12}$ m/s, when $K_{Rep} = 100 \cdot K_{500}$.

- The Darcian velocities in rock near the repository at the depth of 500 m are slightly (less than one decade) increased.

The first variant case:

The pattern of the result is unchanged, only the scale is increased by one decade.

The second variant case (App. 17–20, 24):

As K_{Rep} increases from $1/100 \cdot K_{500}$ to $100 \cdot K_{500}$:

- The value of the Darcian velocity near the ground surface above the repository (q = 0.6·10^{-10} m/s) and the depth (130 m) at which it is dropped to 10 % of this remain unchanged.
- The flow through the repository increases slightly. When $K_{Rep} = 1/100 \cdot K_{500}$, compared to the natural case, on the centre of the repository, the direction of the flow is still straightly downwards but on the sides, the flow is more horizontal. The flow through the repository occurs mostly through the centre of it. When $K_{Rep} = 100 \cdot K_{500}$, on the sides of the repository, the flow is directed almost vertically through the repository both from above and from below (App. 24).
- The range of the Darcian velocity values on the horizontal axis of the repository plate increases gradually from $q \in [0.03, 0.1] \cdot 10^{-15}$ m/s, when $K_{Rep} = 1/100 \cdot K_{500}$ to $q \in [0.06, 0.2] \cdot 10^{-13}$ m/s, when $K_{Rep} = 100 \cdot K_{500}$.

The asymmetry in the result figures (App. 17–20) is due to numerics, e.g. the asymmetry of the calculation mesh for the state with a repository (App. 27).

10.5 Comparison of the results for the natural state and the state with a repository

10.5.1 Linear head

The results for both the natural state and the state with a repository suggest a horizontal flow from the higher head on the right hand side of the domain to the lower head on the left. The flow field does not present any significant maxima. The Darcian velocities are the highest near the ground surface and are dropped to 10 % of that at the depth of 230 m.

When K_{Rep} increases, the flow through the repository increases. When compared to the natural state, the Darcian velocities on the repository segment are ~100 times smaller, when $K_{Rep} = 1/100 \cdot K_{500}$ and ~10 times greater, when $K_{Rep} = 100 \cdot K_{500}$.

10.5.2 Parabolic head

The results for both the natural state and the state with a repository suggest a flow from the higher head in the centre of the ground surface to the lower head in the upper corners of the modelling domain, where maxima of the flow field occur. The Darcian velocity at the depth of 240 m above the repository is 10 % of that near the ground surface.

When K_{Rep} increases, the flow through the repository increases. When compared to the natural state, the Darcian velocities on the repository segment are ~10 times smaller, when $K_{Rep} = 1/100 \cdot K_{500}$ and ~10 times larger, when $K_{Rep} = 100 \cdot K_{500}$.

10.5.3 Cosine-shaped head

The results for both the natural state and the state with a repository suggest a flow from under hills to under valleys with most of the flow occurring near the ground surface. In the base case and in the first variant case, the depth at which the Darcian velocity has dropped to 10 % is 220 m for the natural state and 210 m for the state with a repository. In the second variant case, the depth at which the Darcian velocity has dropped to 10 % is 150 m for the natural state and 130 m for the state with a repository.

When K_{Rep} increases, the flow through the repository increases. In the base case and both the variant cases, when compared to the natural state, the Darcian velocities on the repository segment are ~10 times smaller, when $K_{Rep} = 1/100 \cdot K_{500}$ and ~10 times larger, when $K_{Rep} = 100 \cdot K_{500}$.

10.6 Conclusion of the base cases

10.6.1 General

The used alternative range of the head on the top boundary ($h \in [0, 100]$ m) is unrealistically large but with the help of it, it was obtained, that changing the variation of the absolute values of the prescribed head on the top boundary does not change the shape of the result in any (linear, parabolic or cosine-shaped) case, only the absolute values. In the following conclusions, only the results for the cases, in which the head on the top varies as $h \in [0, 10]$ m are compared to each other.

On the other hand, changing of the frequency of the regional variation of the head (the cosine-shaped case) changes also the shape of the solution. A higher frequency forces the flow to occur nearer the ground surface, whereupon variation of the conductivity of the repository has a smaller effect on the flow pattern.

The influence of a repository to the flow pattern is small and the changes concentrate in the vicinity of the repository.

10.6.2 Flow in the vicinity of the repository

When K_{Rep} increases, the flow through the repository increases and the flow directions around the repository change in every case. The relative change of the Darcian velocities q with K_{Rep} in the linear case is slightly larger than in all the other cases.

In the parabolic case and in the base case of the cosine-shaped condition, the relative change of the flow directions around the repository is essentially the same, although in the cosine-shaped case the change is more apparent because of the larger scale and, consequently, the visible change of the head around the repository (App. 22–23).

All these changes are local concentrating within < 200 m from the repository. In the rock near the repository at the depth of 500 m, the Darcian velocities are only slightly changed in all the cases.

For the cases in the natural state, in which the head on the top varies as $h \in [0, 10]$ m, the largest Darcian velocities on the repository segment vary in the range

$q \in [0.04, 0.5]\cdot10^{-13}$ m/s = $[0.01, 0.2]\cdot10^{-5}$ m/yr.

The largest value of these occurs in the base case of the cosine-shaped condition and the smallest value in the base case of the parabolic condition and in the second variant case of the cosine-shaped condition.

For the cases in the state with a repository for which the head on the top varies as $h \in [0, 10]$ m, the largest Darcian velocities on the repository segment vary in the range

$q \in [0.01, 0.8]\cdot10^{-14}$ m/s = $[0.004, 0.2]\cdot10^{-6}$ m/yr, when $K_{Rep} = 1/100\cdot K_{500}$. The largest value of these occurs in the base case of the cosine-shaped condition and the smallest value in the base case of the linear condition and in the second variant case of the cosine-shaped condition.

When $K_{Rep} = 100\cdot K_{500}$, the range of the largest Darcian velocities on the repository segment is

$q \in [0.02, 0.6]\cdot10^{-12}$ m/s = $[0.007, 0.2]\cdot10^{-4}$ m/yr.

The largest value of these occurs in the base cases of the linear and cosine-shaped conditions and the smallest value in the second variant case of the cosine-shaped condition.

10.6.3 Variation with depth

In the natural case, the depth at which the Darcian velocity has dropped to 10 % of the value near the ground surface above the repository is the smallest, 150 m, in the second variant case of the cosine-shaped condition. In all the other natural cases, the value varies in the range 220–240 m. These values are not affected by a repository.

Changes in the results for the depth calculations were observed for the natural case and the case with a repository for the cosine-shaped condition. The difference is small and partly due to the different calculation meshes.

10.7 Sensitivity cases

So far, the sides and the bottom of the modelling domain have been fixed and supposed to be no-flow boundaries in this study. To briefly consider other kinds of assumptions on these boundaries, these conditions are varied in the parabolic top

boundary case in the natural state. The studied variants are:

- expansion of the side boundaries of the domain and
- assignment of a linearly declining head at the bottom boundary.

The results of one case of each are illustrated in Appendices 25 and 26.

10.7.1 Side boundary expansion

As the side borders are expanded, the general flow pattern is essentially the same as in the base case of the parabolic condition for the natural state (App. 2). In the vicinity of the repository segment, the flow pattern is unchanged. The largest difference occurs naturally near the original side boundaries ($x = \pm 3150$ m), where the no-flow condition does not exist any more. The Darcian velocities at the reference points are slightly smaller than in the base case.

When the sides are at $x = \pm 5000$ m (App. 25), the parabolic top boundary condition is $h = -x^2/2500000 + 10$ m ($h \in [0, 10]$ m). The largest values of the Darcian velocity, $q = 0.5 \cdot 10^{-11}$ m/s, occur near the upper corners of the domain. The range of the values of Darcian velocity on the repository segment is $q \in [0.02, 0.7] \cdot 10^{-15}$ m/s with the smallest values occurring in the edges and the largest in the centre of the segment. Near the ground surface above the repository segment, the Darcian velocity is $q = 0.9 \cdot 10^{-13}$ m/s and drops to 10 % of this approximately at the depth of 270 m.

10.7.2 Linear head at the bottom

When a linear head is assigned at the bottom of the domain, the head field and the general flow pattern in the part of the domain from the ground surface to the depth of ~1000 m are essentially the same as in the base case of the parabolic condition for the natural state (App. 2). In the vicinity of the repository segment, the flow pattern is unchanged. The values of Darcian velocity at the reference points are not changed.

When the linear head at the bottom is $h = 5 + x/630$ m ($h \in [0, 10]$ m) (App. 26), the largest values of the Darcian velocity, $q = 0.9 \cdot 10^{-11}$ m/s, occur near the upper corners of the domain. The range of the values of Darcian velocity on the repository segment is $q \in [0.1, 0.4] \cdot 10^{-14}$ m/s. Near the ground surface above the repository segment, the Darcian velocity is $q = 0.2 \cdot 10^{-12}$ m/s and drops to 10 % of this approximately at the depth of 240 m.

11 CONCLUSION AND DISCUSSION

When selecting a location for a repository, the interest would be to find conditions, where the flow through the repository is small and directed away from the biosphere. Accordingly, favourable features for the system are e.g.

- a small variation of the absolute value and a high frequency of the regional variation of the head on the top of the model as well as
- small conductivity of the repository K_{Rep} and
- the location of the repository under a hill.

In any case, the influence of a repository to the flow pattern is small, especially when some or all of the conditions above are true. Furthermore, the changes concentrate in the vicinity of the repository.

The assumptions and simplifications in the calculations of this study included e.g.

- the EC model was used, in which the 2-dimensional domain was considered a continuum of equivalent properties without fractures present,
- the calculations were done for stationary fields, without sources or sinks present in the domain and with a constant density of the ground water,
- the repository was represented by a 2-dimensional, isotropic plate, the conductivity of which was given fictitious values,
- the hydraulic conductivity of rock was supposed to have an exponential depth dependence,
- the elevation of the water table was fixed and varied with the topography of the ground surface.

The simplified model and geometry for the problem were used to give qualitative information on the groundwater flow in bedrock as well as of the orders of magnitude of the physical quantities. The hydraulic conductivity of intact rock is well known to reduce with depth but the used mathematical dependence [9] is not obvious. The real natural conditions are not fixed and stationary, and they can be considerably disturbed by excavation e.g. by changing the water table elevation.

The calculations were performed with the Matlab® Partial Differential Equation Toolbox, whose approach to create meshes and to do the calculations were not looked into in this study. Unsymmetry is found in some of the results, but in general, the results for different geometries are consistent and of the same order of magnitude as in other studies.

In [8], a flow field is calculated with the FEFLOW-code for the Olkiluoto site 500 years after the sealing of the repository. The Darcian velocity values on the repository plate are approximately in the range $q \in [10^{-4}, 10^{-2}]$ m/yr. In the rock around the repository, the values are smaller in the range $q \in [10^{-8}, 10^{-4}]$ m/yr. The Darcian velocities in the rock are approximately of the same order of magnitude as in the results of this study, but the values for the repository are ~10–1000 times larger compared to the results for the case in which $K_{Rep} = 100 \cdot K_{500}$. The main reasons for the difference are the selection of the size, geometry and conductivity parameters for the plate representing the repository and the fact that the results in [8] are calculated for a 3-dimensional situation.

Expansion of the side boundaries seems to reduce the flow throughout the modelling domain, which is reasonable. The changes are the smallest in the central portion of the domain, where the repository is located. Linear head at the bottom, which resembles a large, declining and highly transmissive fracture zone below the bottom of

the model, does not have an influence on the flow conditions in the main portion of the modelling domain.

The variation of the conceptual boundary conditions on the vertical sides of a modelling domain would also be an interesting area of research. Generally, the Finnish approach of assigning a no-flow condition, which prevails along the whole thousands of meters deep side is very simplified. On the contrary, in a Swedish study the basic condition was a prescribed head on a landward side boundary. An exact specification and justification of this kind of condition for the whole range of a side boundary is a complex task and could be a subject for a more detailed study.

REFERENCES

[1] Swedish Nuclear Power Inspectorate: SKI SITE-94 Deep Repository Performance Assessment Project, Volume I. Norstedts Tryckeri AB, Stockholm 1997.

[2] Swedish Nuclear Power Inspectorate: SKI SITE-94 Deep Repository Performance Assessment Project, Volume II. Norstedts Tryckeri AB, Stockholm 1997.

[3] Veikko Taivassalo, Lasse Koskinen, Kurt Meling: Groundwater flow analyses in preliminary site investigations–Modelling strategy and computer codes. Report YJT-94-04, Nuclear Waste Commission of Finnish Power Companies, Espoo 1994.

[4] Veikko Taivassalo, Arja Saarenheimo: VLJ-luolan pohjavesivirtausten analysointi. Raportti YJT-91-10, Nuclear Waste Commission of Finnish Power Companies, 1991.

[5] Jari Löfman, Veikko Taivassalo: FEFLOW 1.10 virtaus-, lämmönsiirto- ja kulkeutumisyhtälöiden ratkaiseminen kytketysti. Raportti YJT-93-30, Nuclear Waste Commission of Finnish Power Companies, Espoo 1993.

[6] Veikko Taivassalo, Antti Poteri: Assessing the velocity of the groundwater flow in bedrock fractures. Report YJT-94-17, Nuclear Waste Commission of Finnish Power Companies, Espoo 1994.

[7] Veikko Taivassalo, Ferenc Meszaros: Simulation of the groundwater flow of the Kivetty area. Report YJT-94-03, Nuclear Waste Commission of Finnish Power Companies, Espoo 1994.

[8] Timo Vieno, Henrik Nordman: Interim report on safety assessment of spent fuel disposal TILA-96. POSIVA-96-17, Posiva Oy, Helsinki 1996.

[9] Jari Löfman: Groundwater flow modelling at the Olkiluoto site–Flow under natural conditions. Work report PATU-96-76e, Posiva Oy, Helsinki 1996.

[10] Lasse Koskinen: Olkiluodon tutkimusalueen pohjavesivirtausten simulointi Virtausmallin säätö ja tulokset. TVO/Paikkatutkimukset, Työraportti 92-83, Teollisuuden Voima Oy, Helsinki 1992.

[11] Jacob Bear: Hydraulics of Groundwater. McGraw-Hill Inc., USA 1979.

[12] Ilmo Kukkonen, Kim Pingoud: Kallion radiogeenisen lämmöntuoton vaikutus pohjaveden virtaukseen. Geologian tutkimuskeskus, Ydinjätteiden sijoitustutkimukset, Tiedonanto YST-55, Espoo, 1987.

[13] Jacob Bear, Arnold Verruijt: Modeling Groundwater Flow and Pollution. D. Reidel Publishing Company, Dordrecht, Holland 1987.

[14] Jari Löfman, Veikko Taivassalo: Simulation of Pressure and Salinity Fields at Äspö. Swedish Nuclear Fuel and Waste Management Co. (SKB), International Cooperation Report 95-01.

[15] E.C. Zachmanoglou, Dale W. Thoe: Introduction to Partial Differential Equations with Applications. Dover Publications, Inc., New York 1986.

[16] O. Lehn Franke, Thomas E. Reilly, Gordon D. Bennett: Definition of boundary and initial conditions in the analysis of saturated ground-water flow systems–an introduction. Techniques of Water-Resources Investigations of the United States Geological Survey, United States Government Printing Office, Washington, 1987.

[17] Lasse Koskinen, Kurt Meling: Numerical study on the effects of the alternative structure geometries on the groundwater flow at the Romuvaara site. Report YJT-94-18, Nuclear Waste Commission of Finnish Power Companies, Espoo 1994.

NATURAL STATE: LINEAR HEAD, THE BASE CASE **APPENDIX 1**

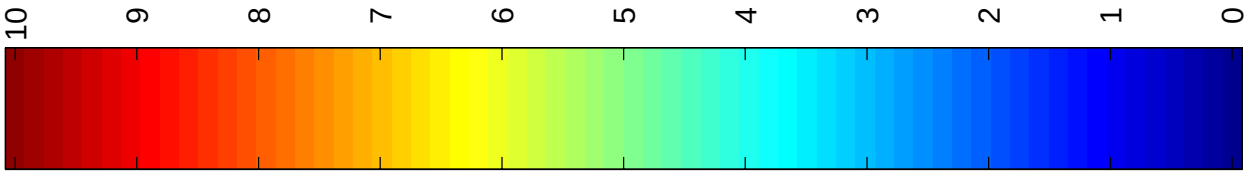

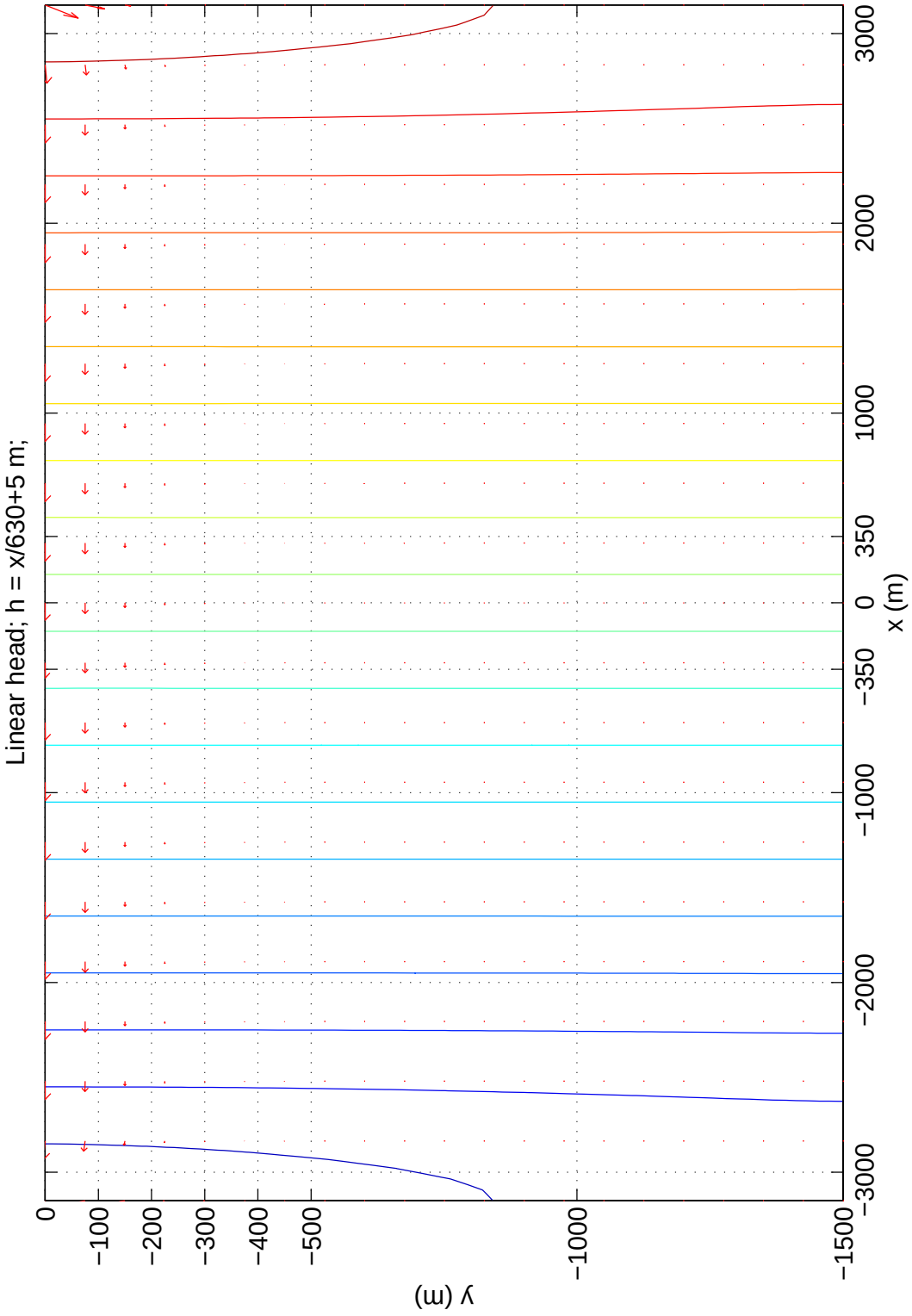

APPENDIX 2 NATURAL STATE: PARABOLIC HEAD, THE BASE CASE

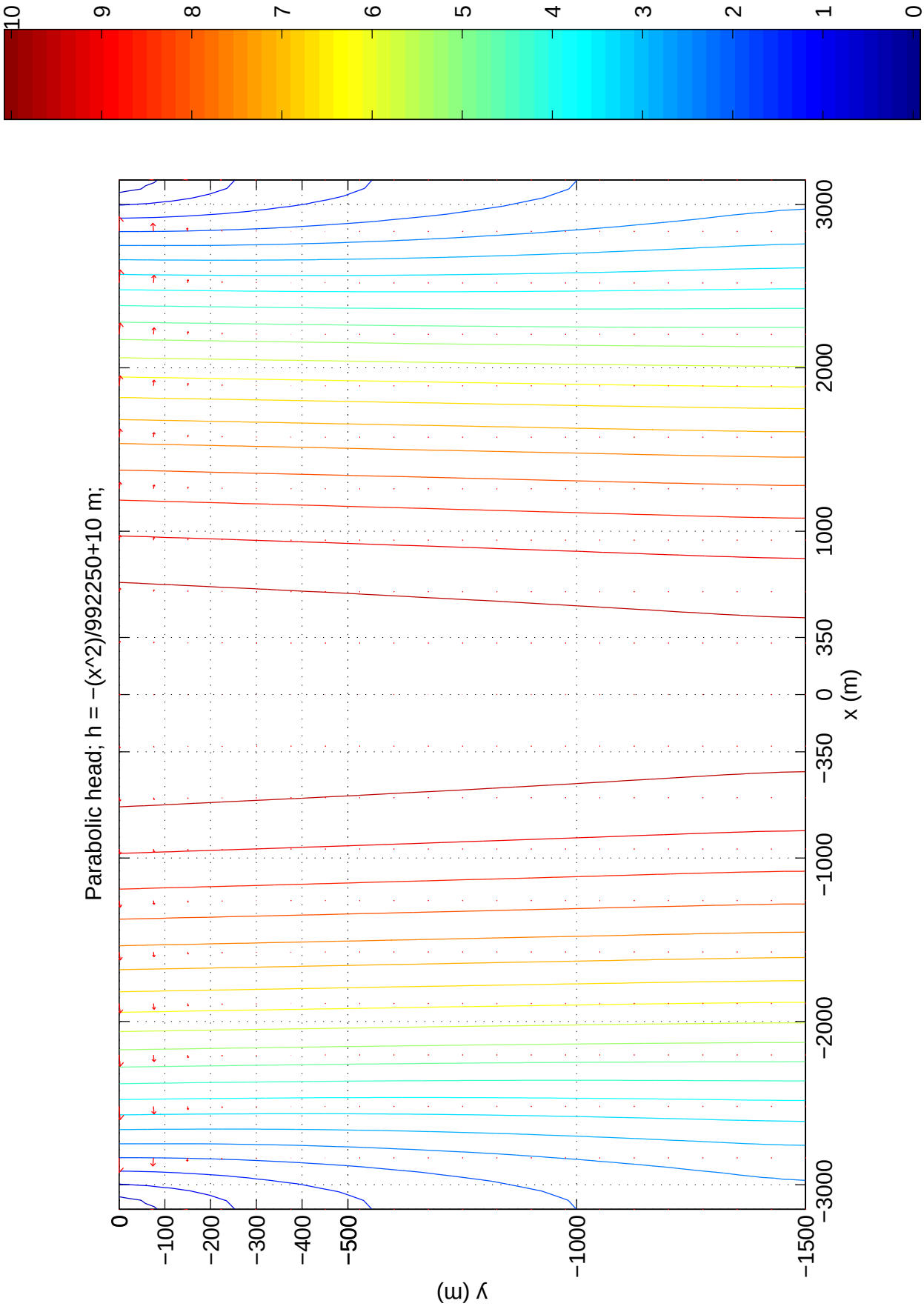

NATURAL STATE: COSINE-SHAPED HEAD, THE BASE CASE **APPENDIX 3**

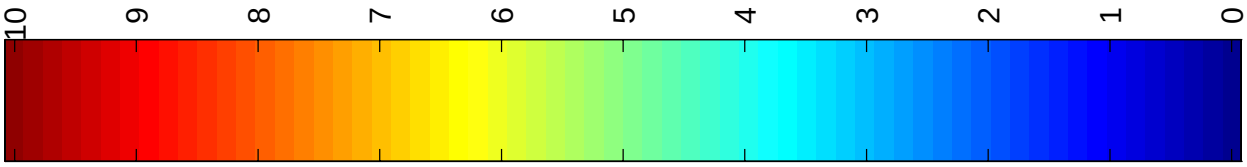

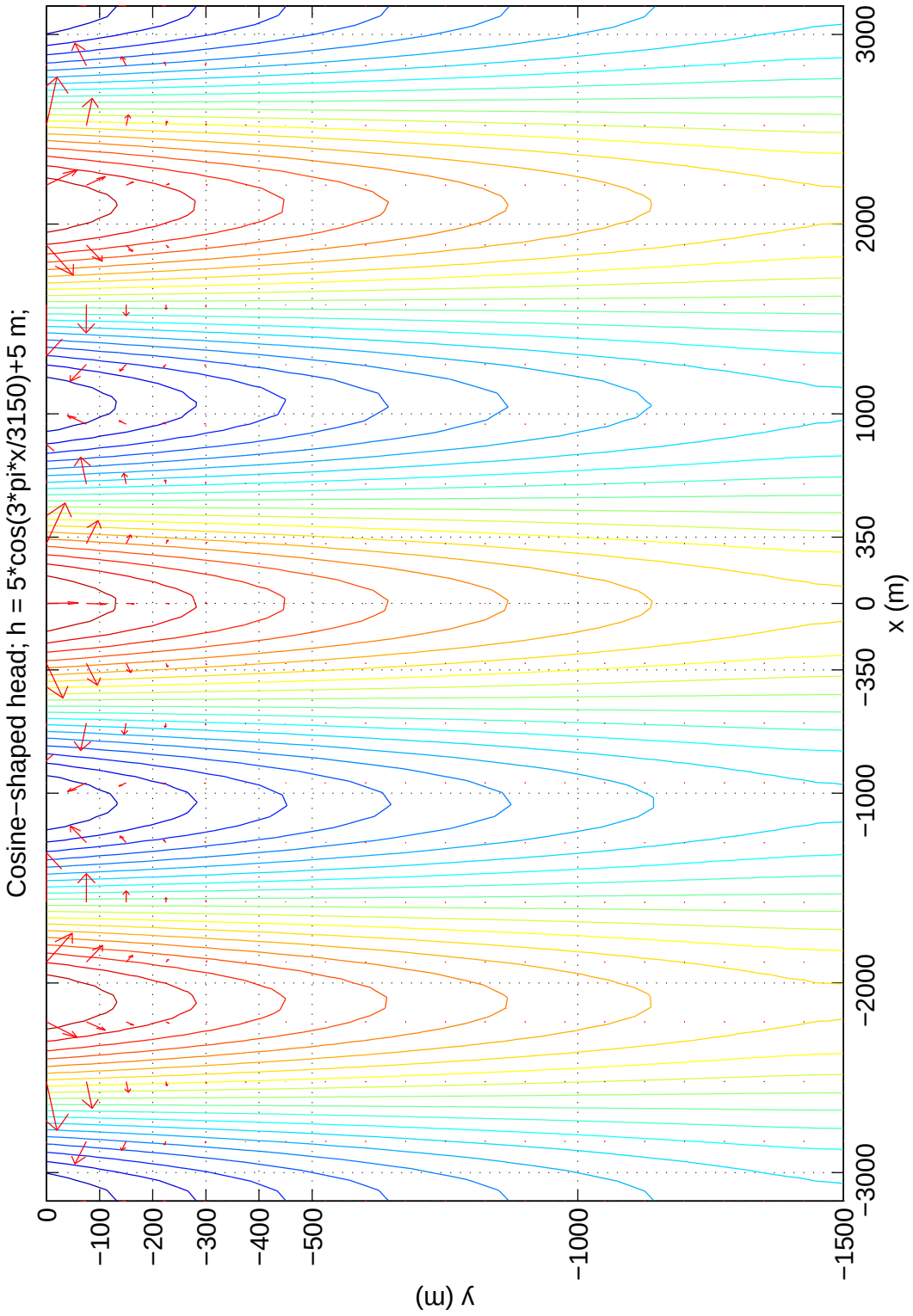

APPENDIX 4 NATURAL STATE: COSINE-SHAPED HEAD, THE SECOND VARIANT CASE

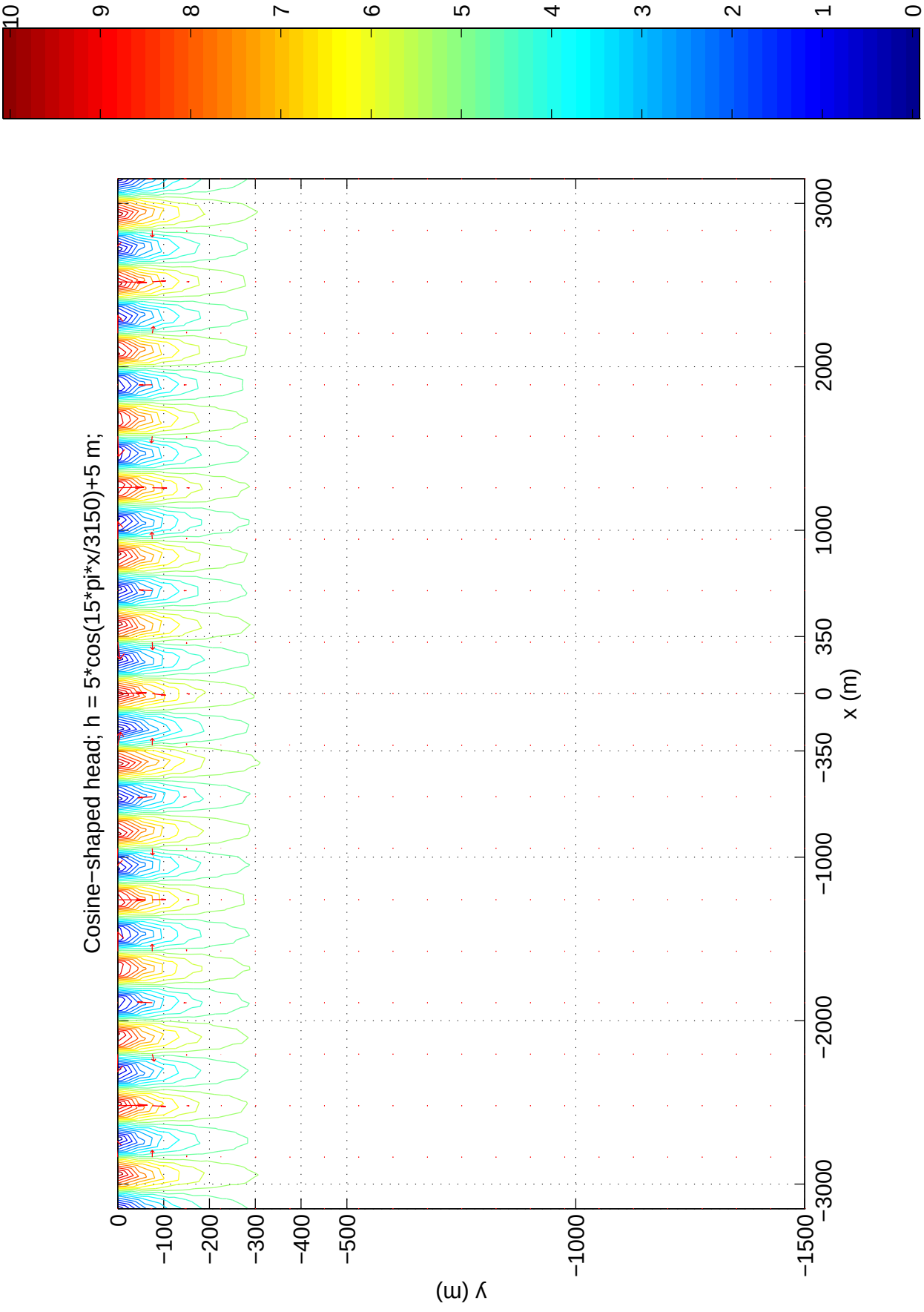

STATE WITH A REPOSITORY: LINEAR HEAD, THE BASE CASE, $K_{Rep} = 1/100 \cdot K_{500}$ **APPENDIX 5**

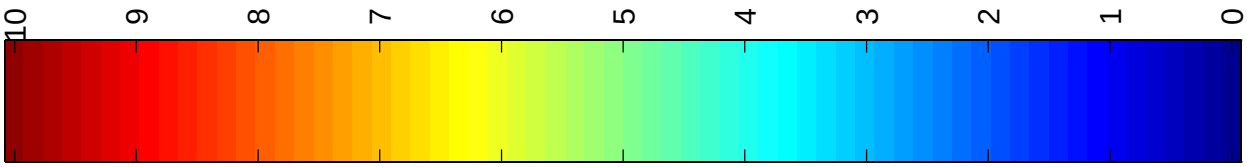

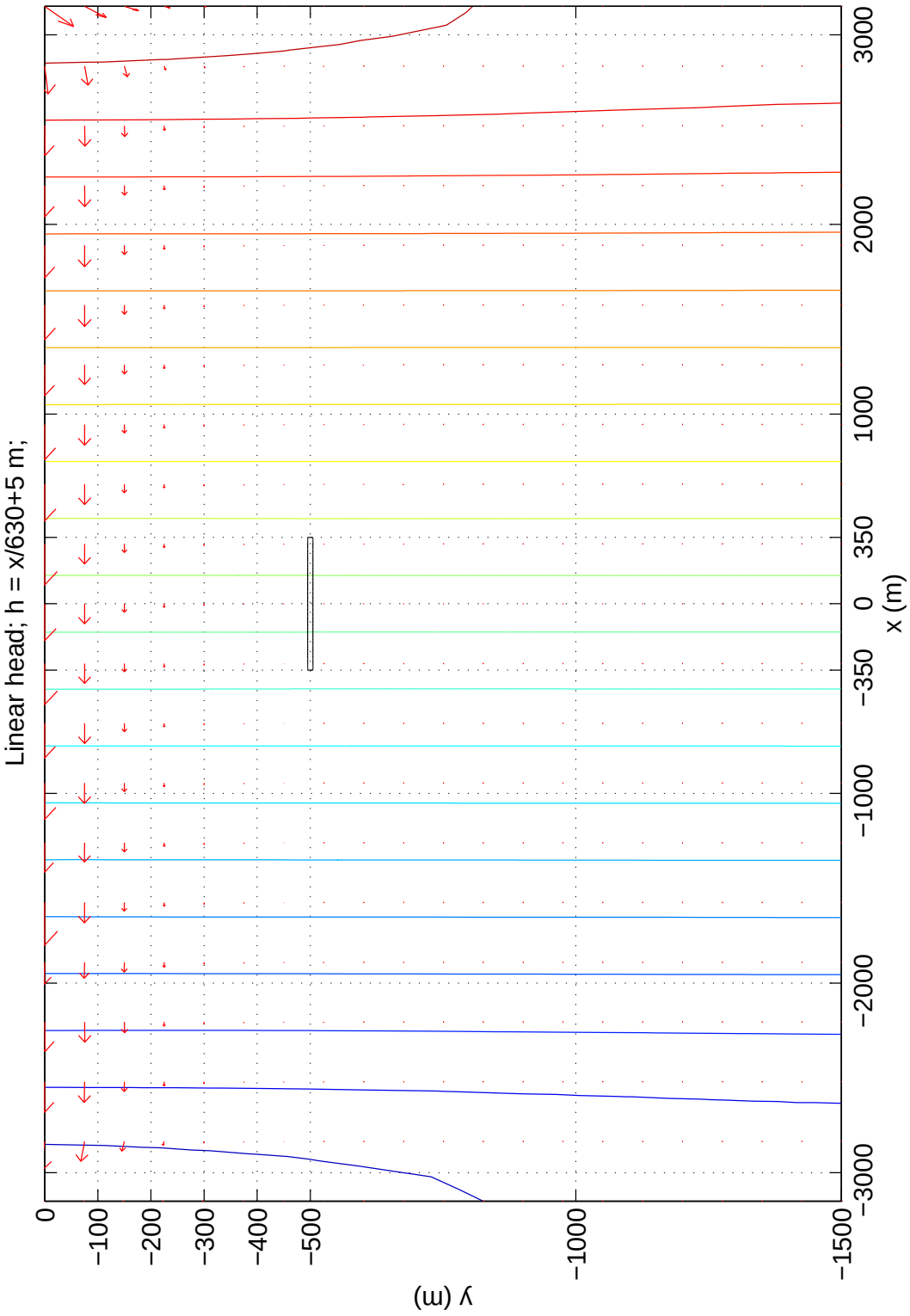

APPENDIX 6 STATE WITH A REPOSITORY: LINEAR HEAD, THE BASE CASE, $K_{Rep} = 1/10 \cdot K_{500}$

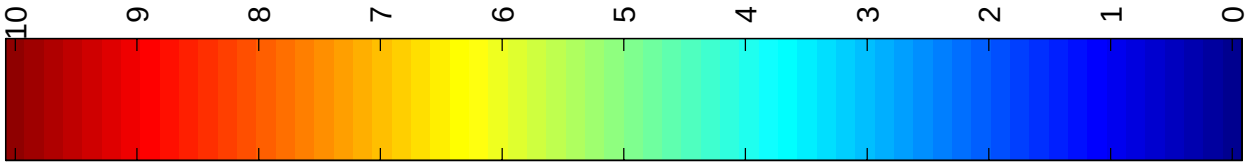

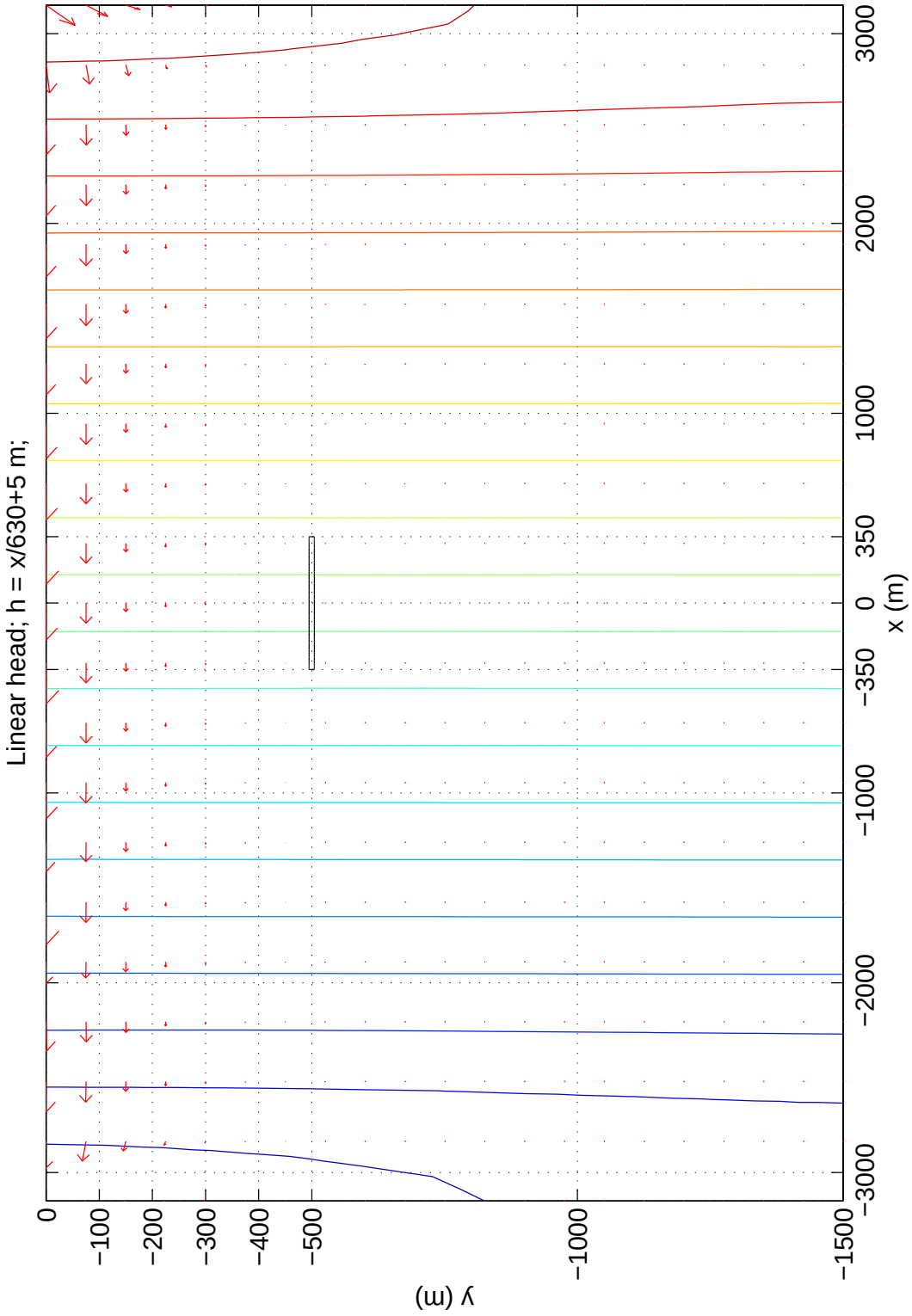

STATE WITH A REPOSITORY: LINEAR HEAD, THE BASE CASE, $K_{Rep} = 10 \cdot K_{500}$ **APPENDIX 7**

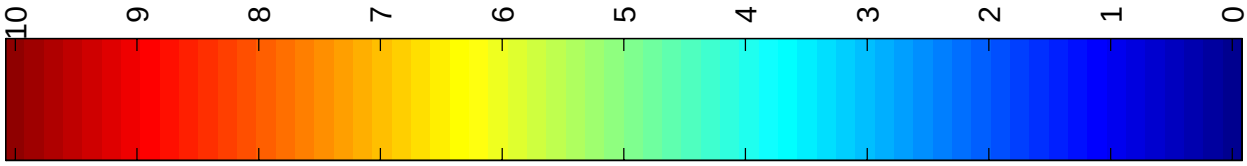

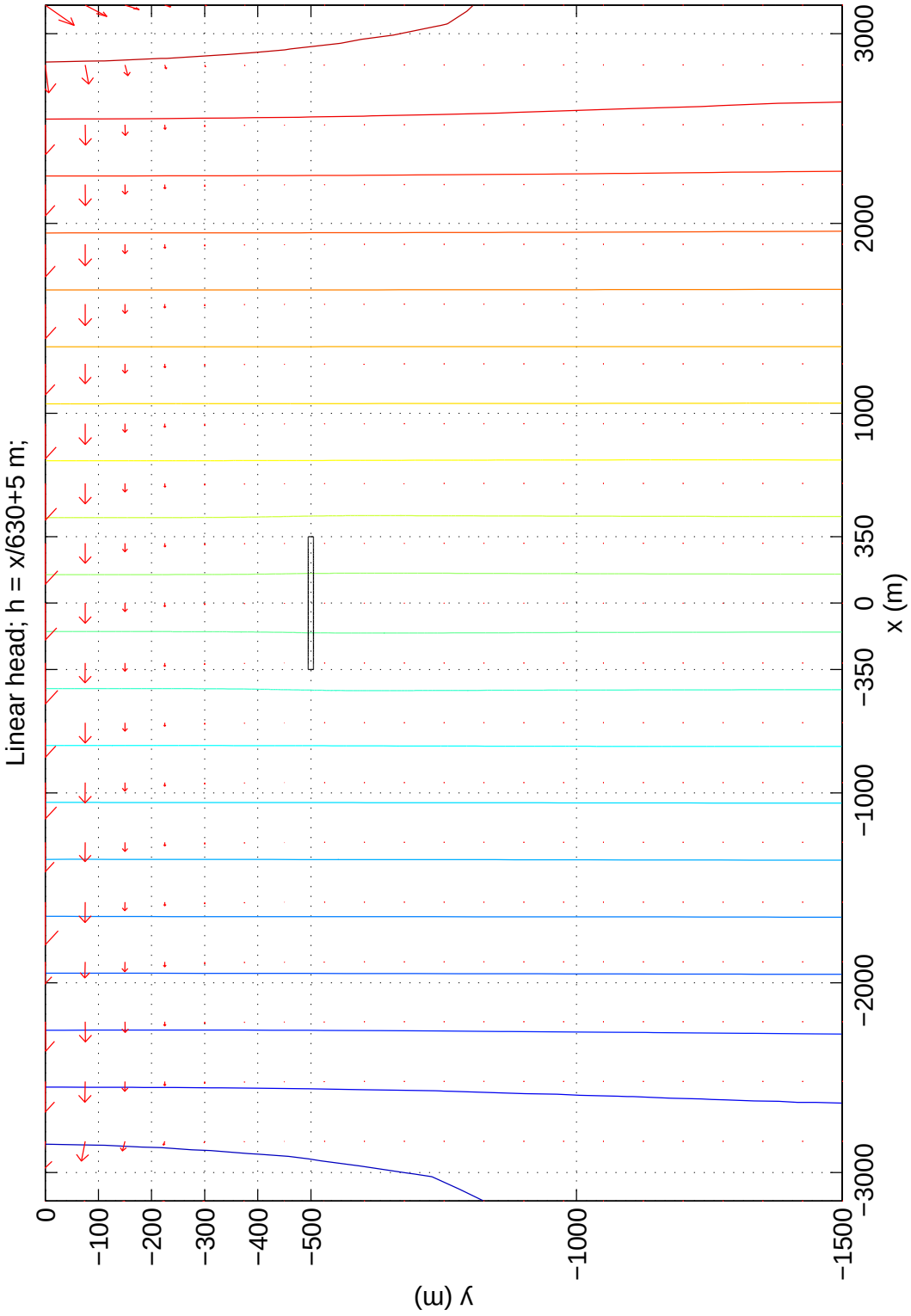

APPENDIX 8 STATE WITH A REPOSITORY: LINEAR HEAD, THE BASE CASE, $K_{Rep} = 100 \cdot K_{500}$

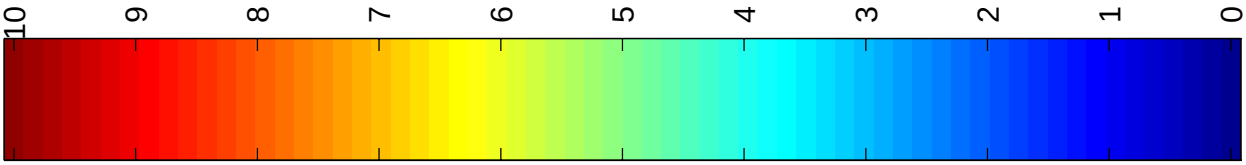

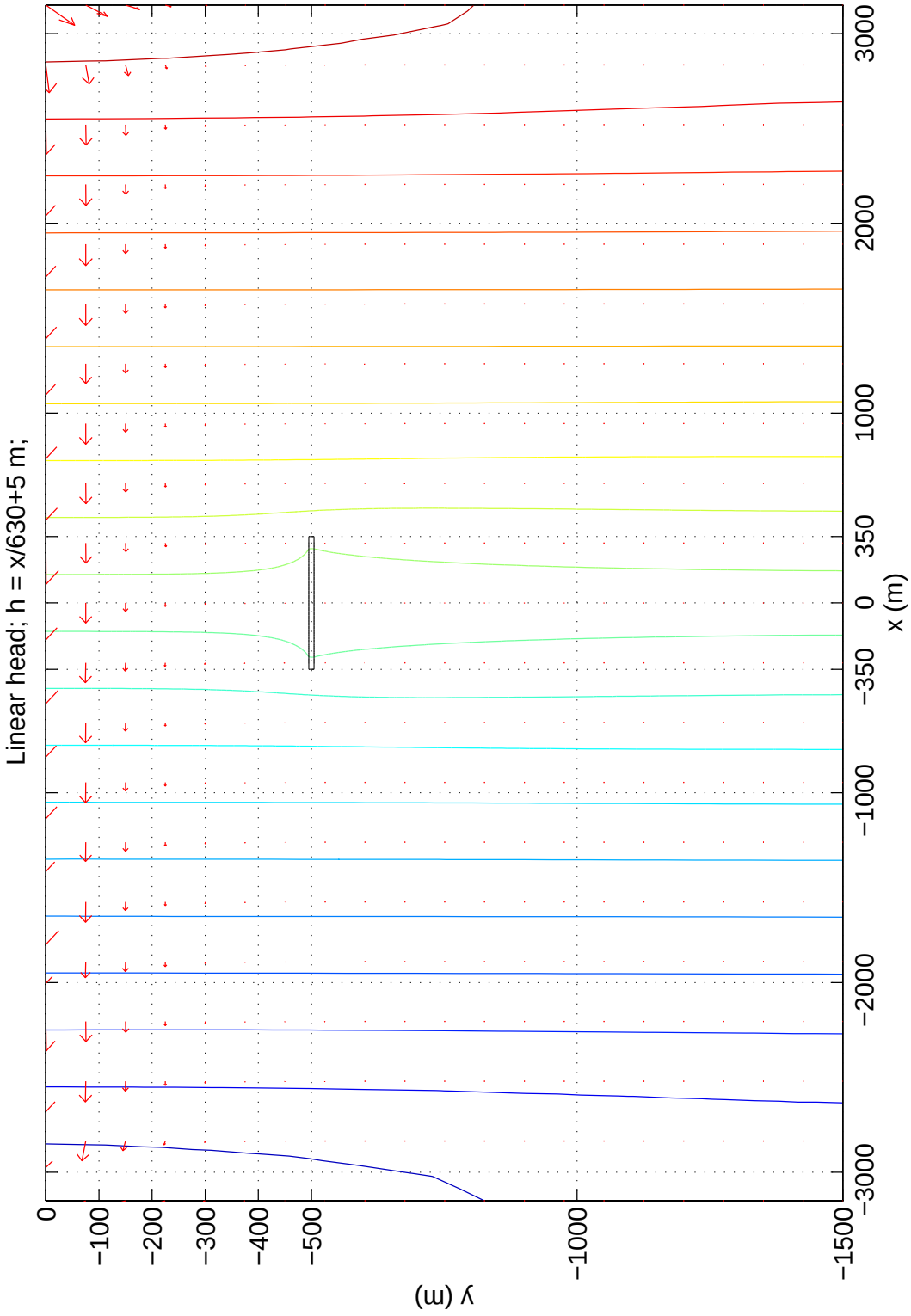

STATE WITH A REPOSITORY: PARABOLIC HEAD, THE BASE CASE, $K_{Rep} = 1/100 \cdot K_{500}$ **APPENDIX 9**

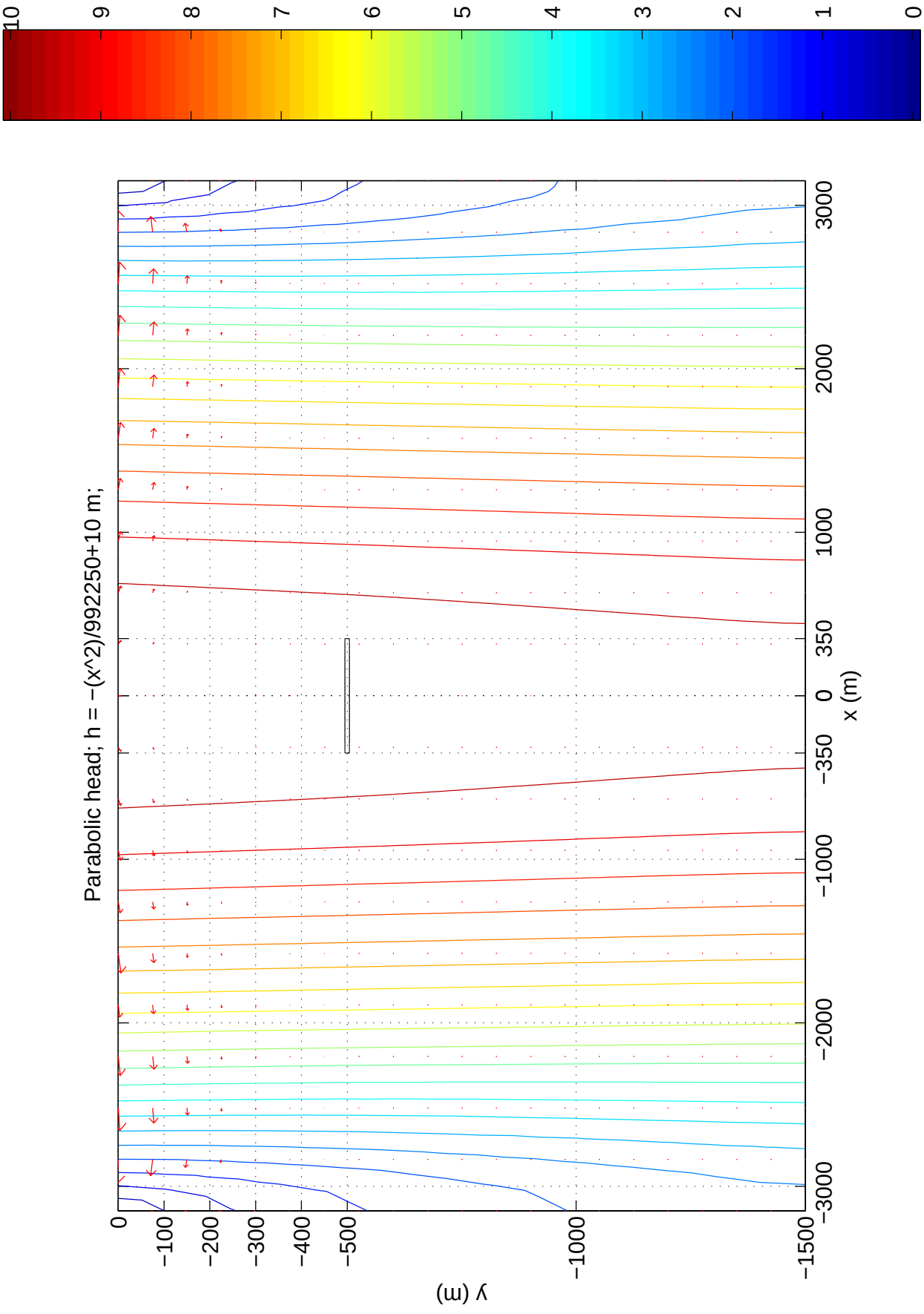

APPENDIX 10 STATE WITH A REPOSITORY: PARABOLIC HEAD, THE BASE CASE, $K_{Rep} = 1/10 \cdot K_{500}$

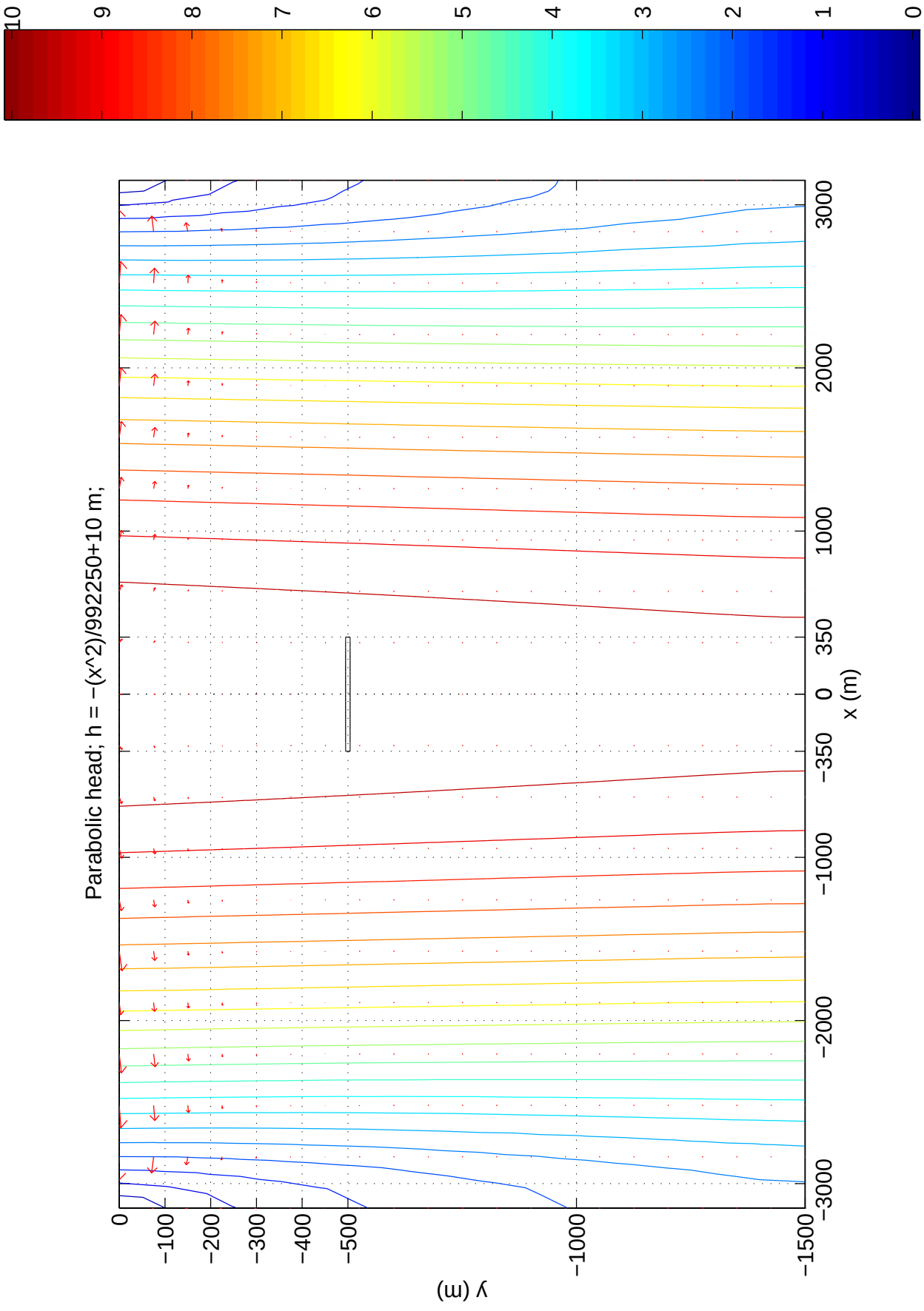

STATE WITH A REPOSITORY: PARABOLIC HEAD, THE BASE CASE, $K_{Rep} = 10 \cdot K_{500}$ **APPENDIX 11**

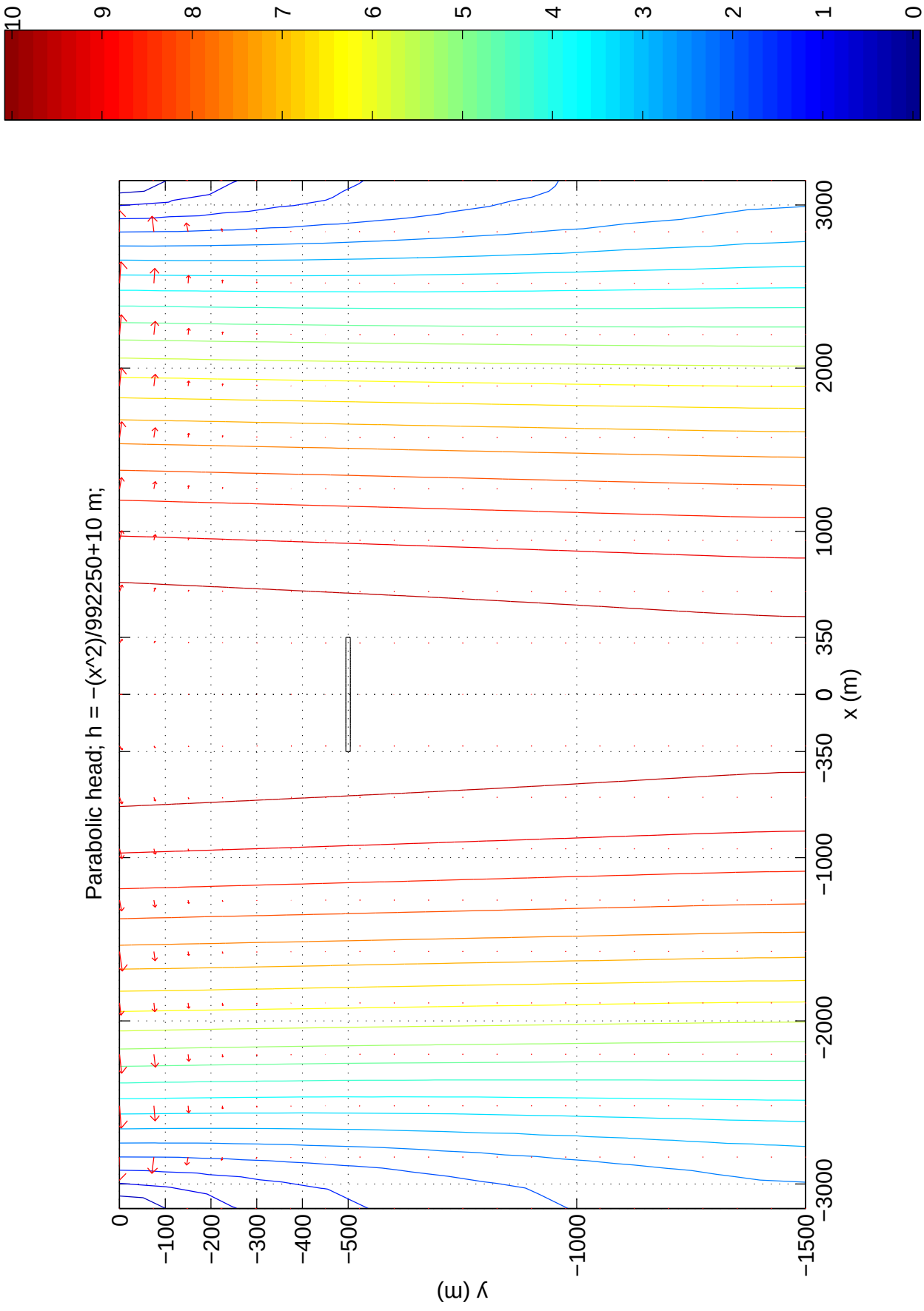

APPENDIX 12 STATE WITH A REPOSITORY: PARABOLIC HEAD, THE BASE CASE, $K_{Rep} = 100 \cdot K_{500}$

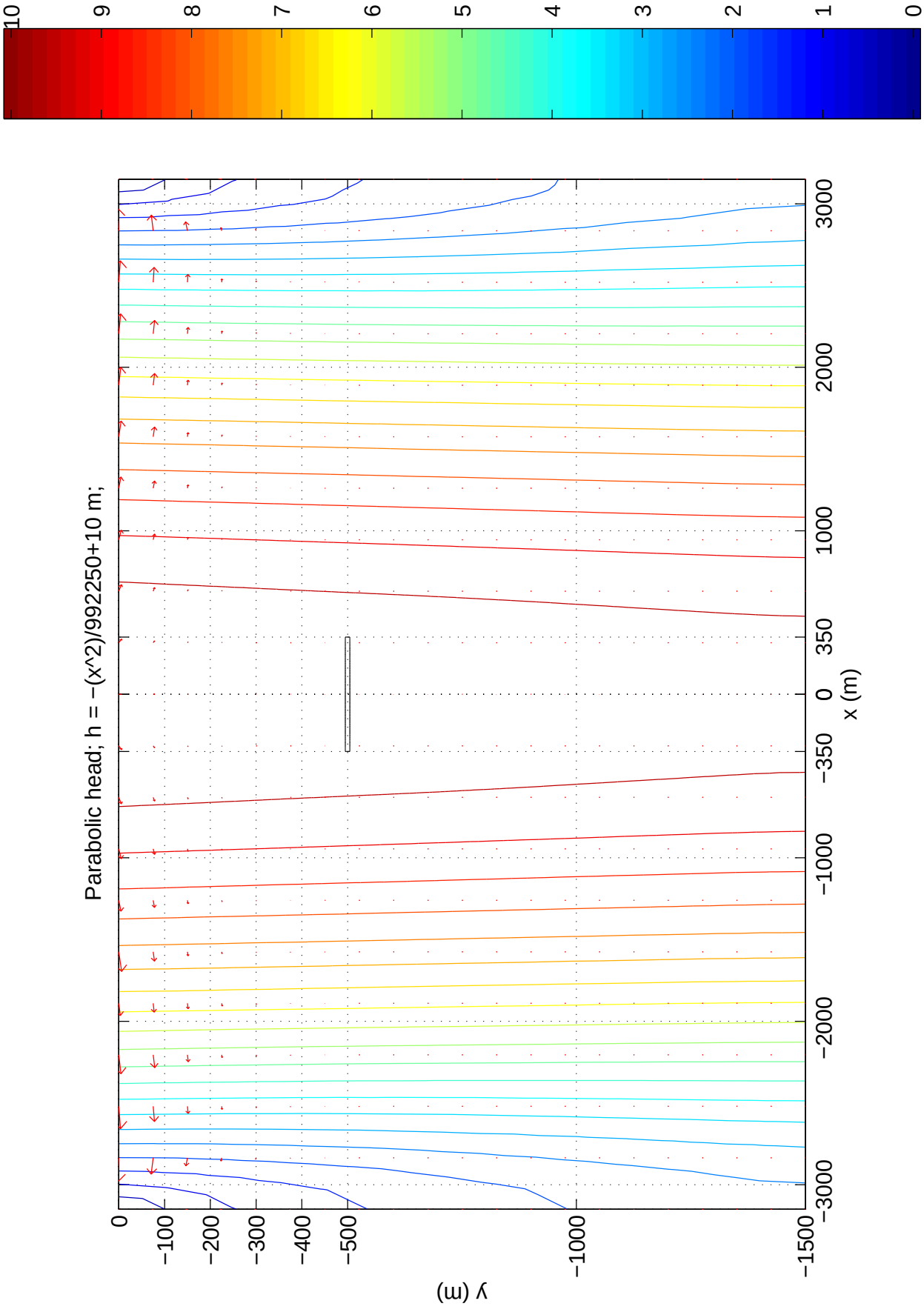

STATE WITH A REPOSITORY: COSINE-SHAPED HEAD, THE BASE CASE, $K_{Rep} = 1/100 \cdot K_{500}$ **APPENDIX 13**

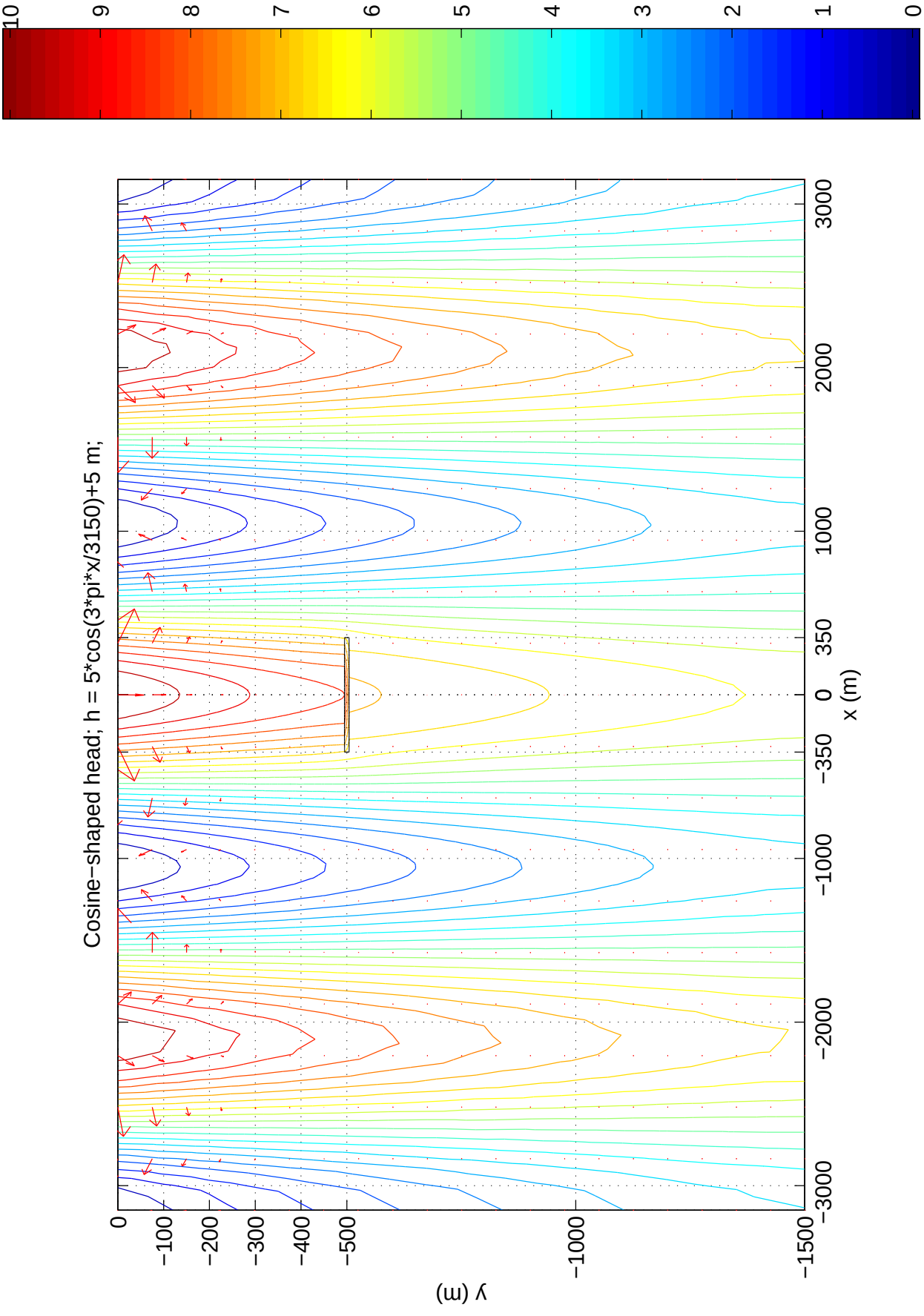

APPENDIX 14 STATE WITH A REPOSITORY: COSINE-SHAPED HEAD, THE BASE CASE, $K_{Rep} = 1/10 \cdot K_{500}$

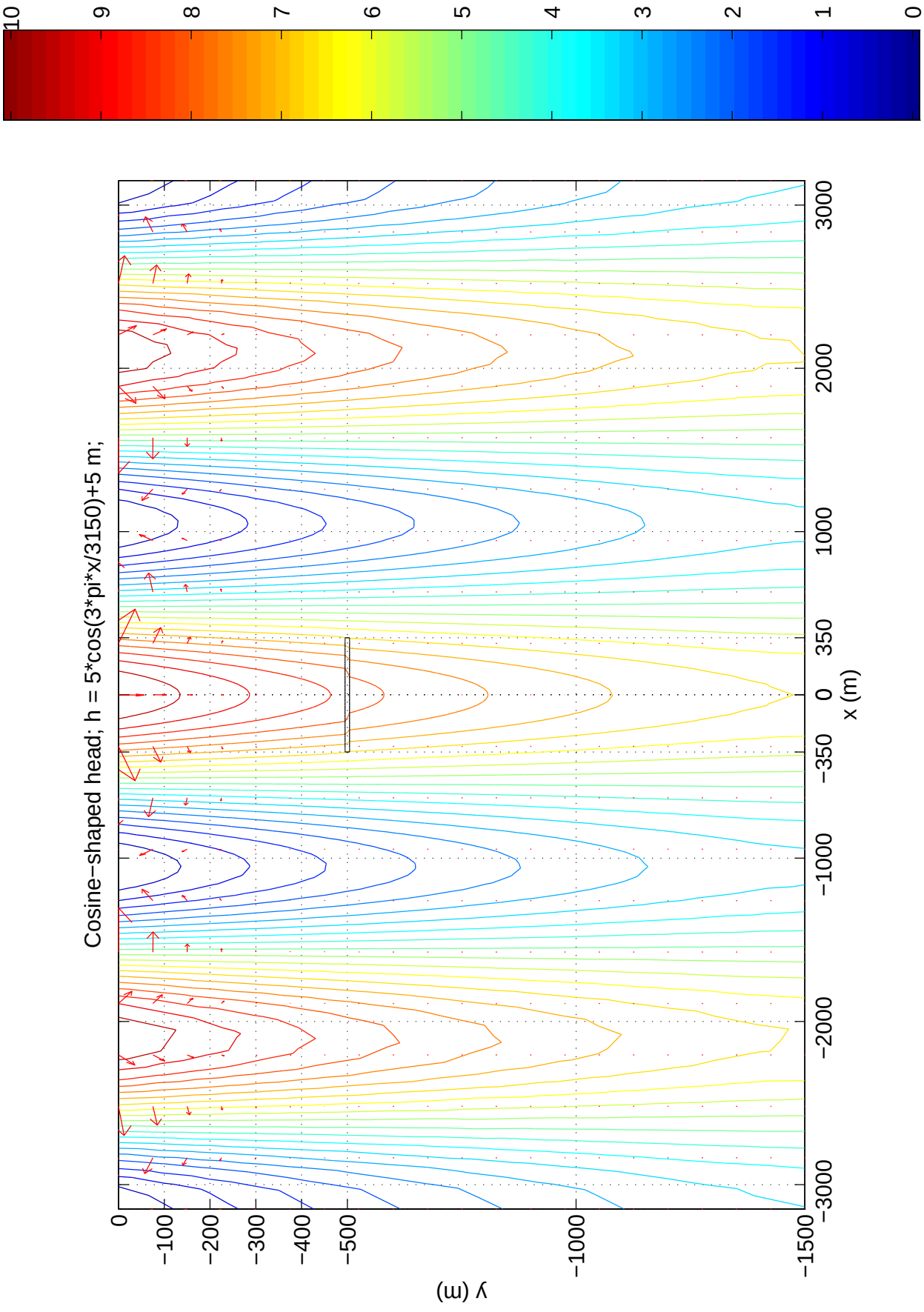

STATE WITH A REPOSITORY: COSINE-SHAPED HEAD, THE BASE CASE, $K_{Rep} = 10 \cdot K_{500}$ **APPENDIX 15**

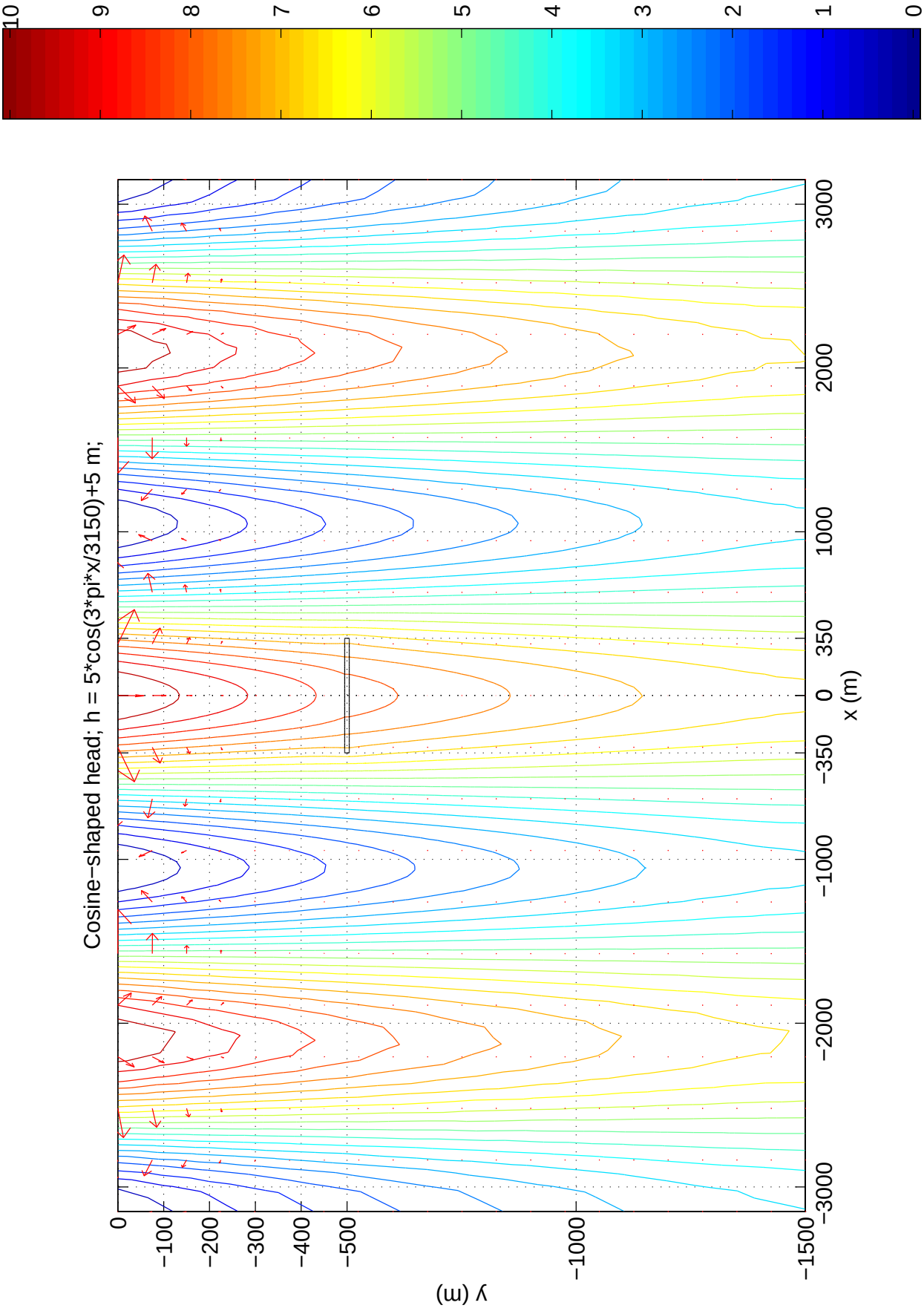

APPENDIX 16 STATE WITH A REPOSITORY: COSINE-SHAPED HEAD, THE BASE CASE, $K_{Rep} = 100 \cdot K_{500}$

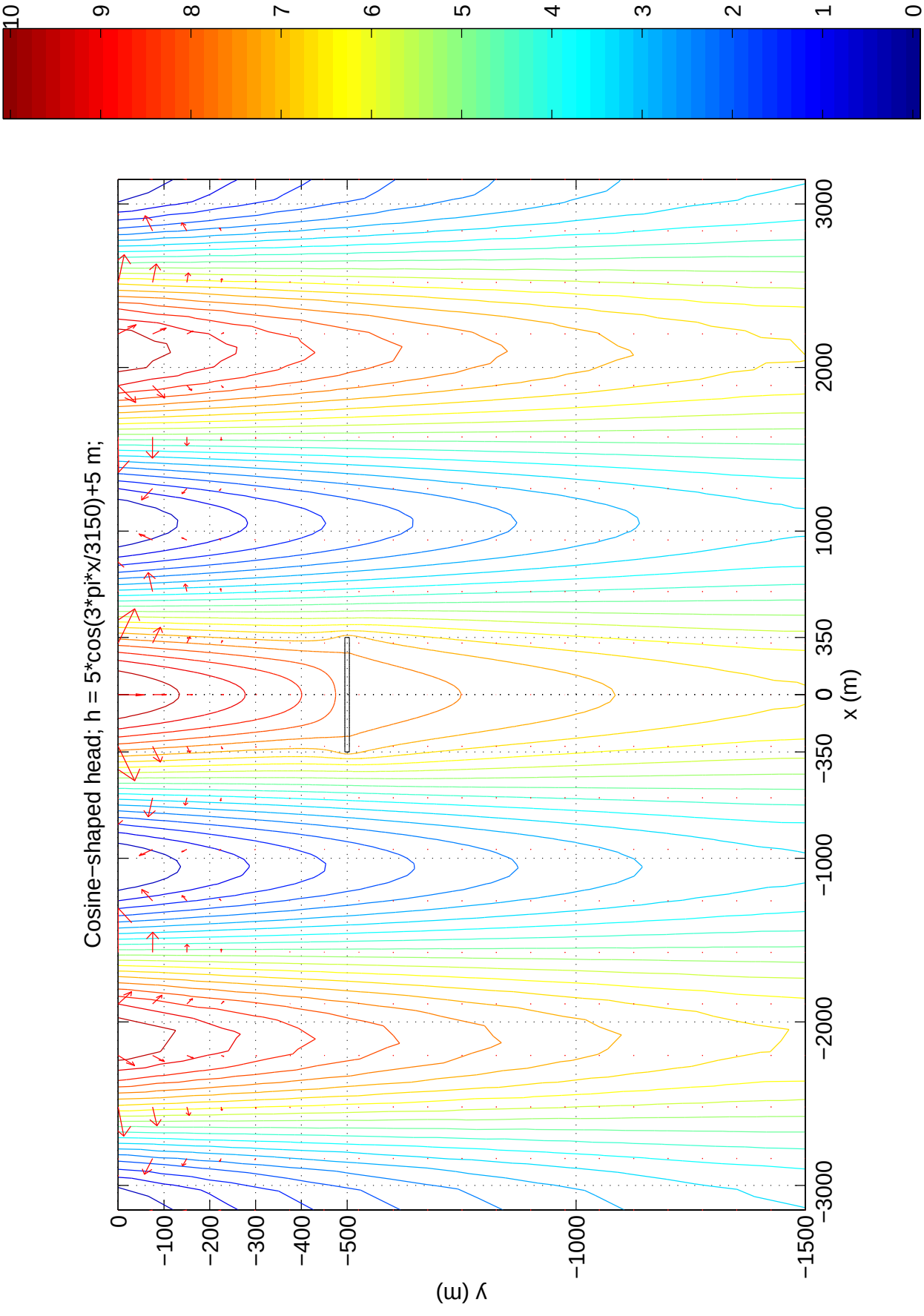

STATE WITH A REPOSITORY: COSINE-SHAPED HEAD, THE SECOND VARIANT CASE, K_{Rep} = 1/100·K_{500} **APPENDIX 17**

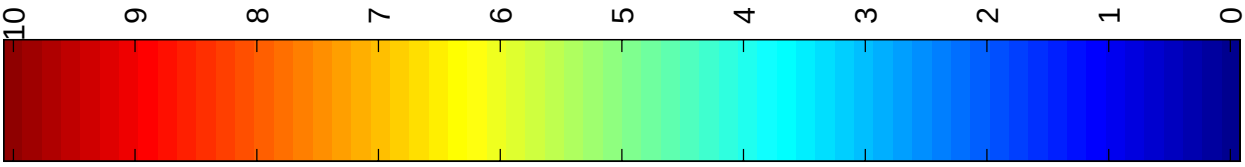

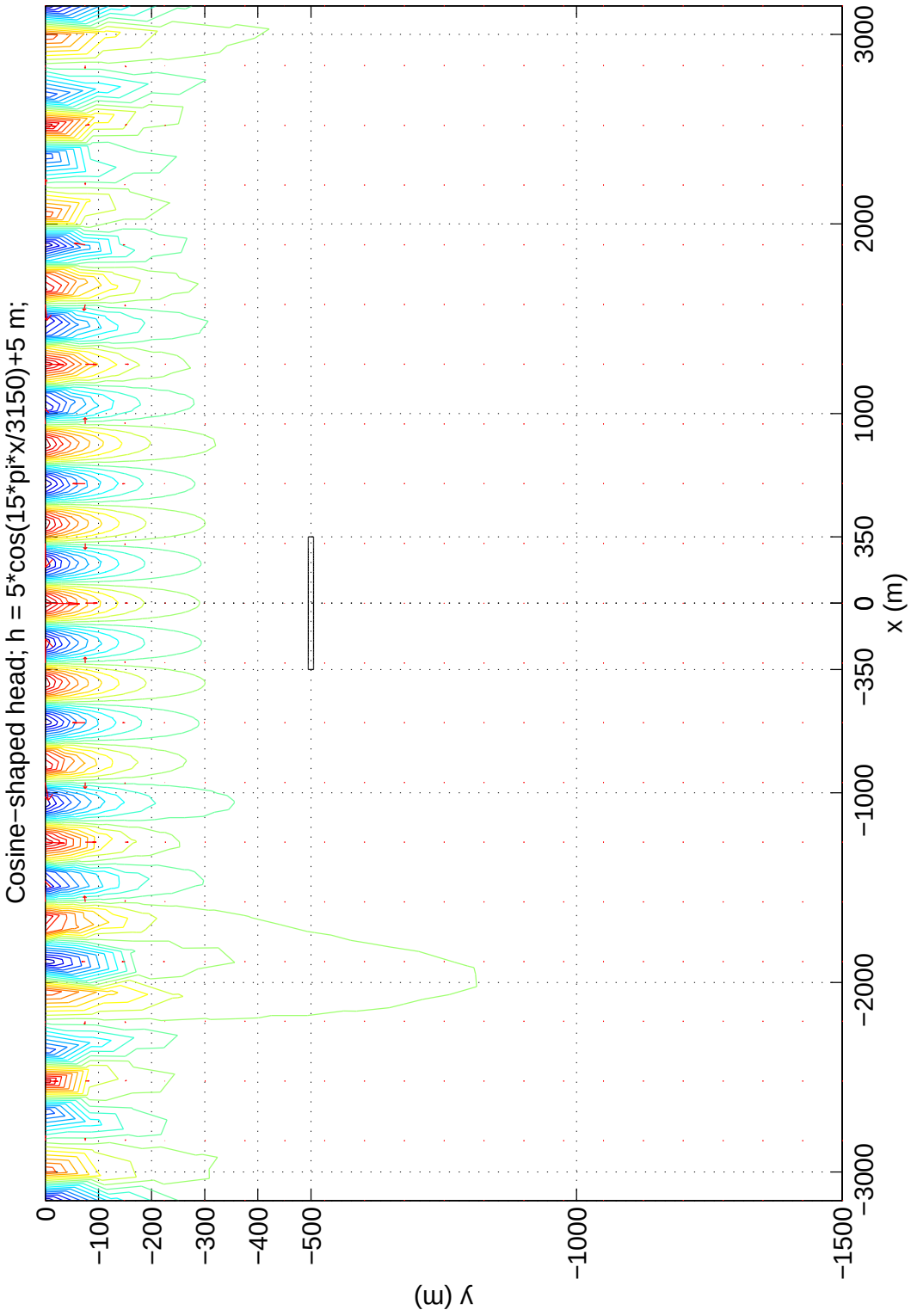

APPENDIX 18 STATE WITH A REPOSITORY: COSINE-SHAPED HEAD, THE SECOND VARIANT CASE, $K_{Rep} = 1/10 \cdot K_{500}$

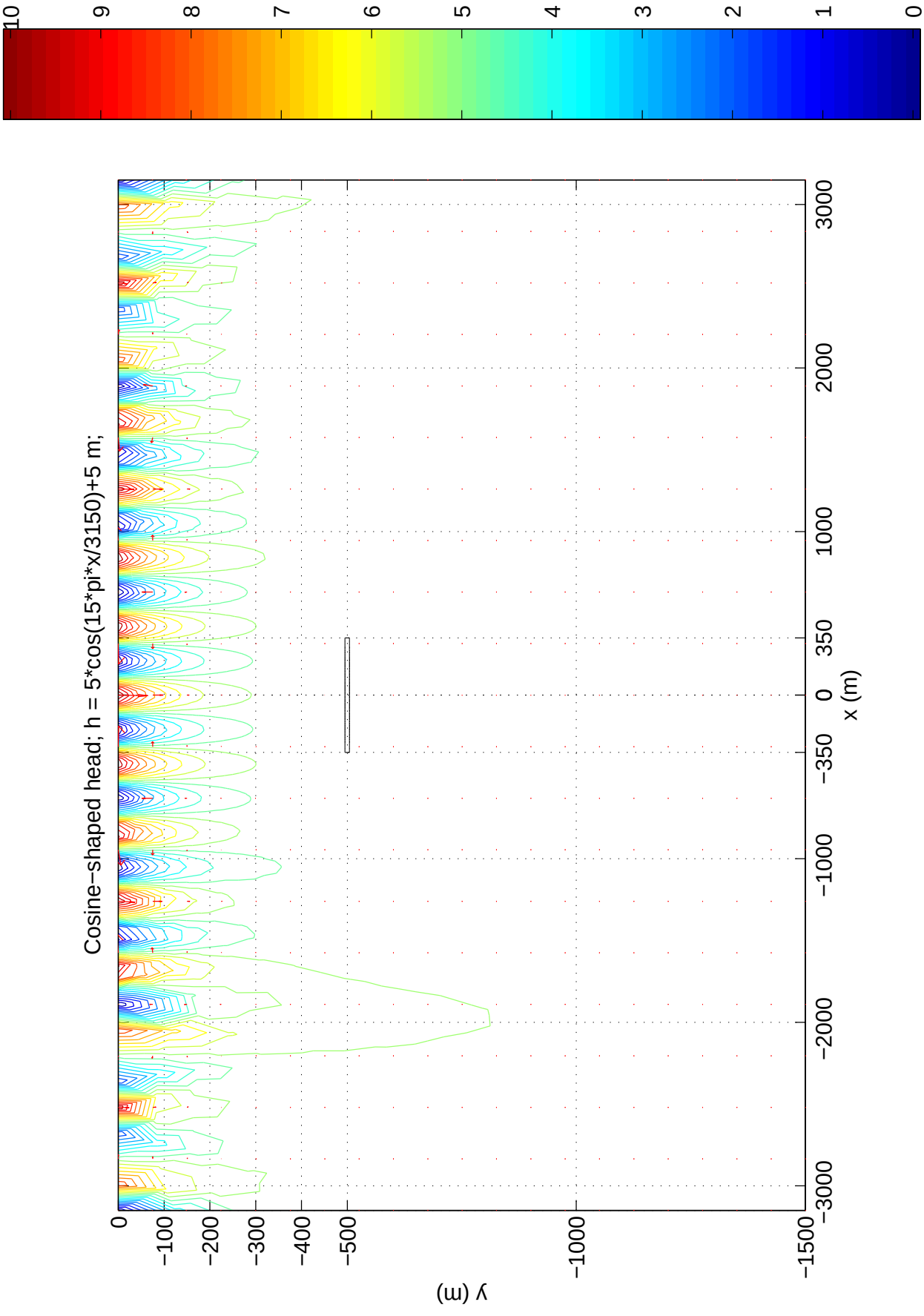

STATE WITH A REPOSITORY: COSINE-SHAPED HEAD, THE SECOND VARIANT CASE, $K_{Rep} = 10 \cdot K_{500}$ **APPENDIX 19**

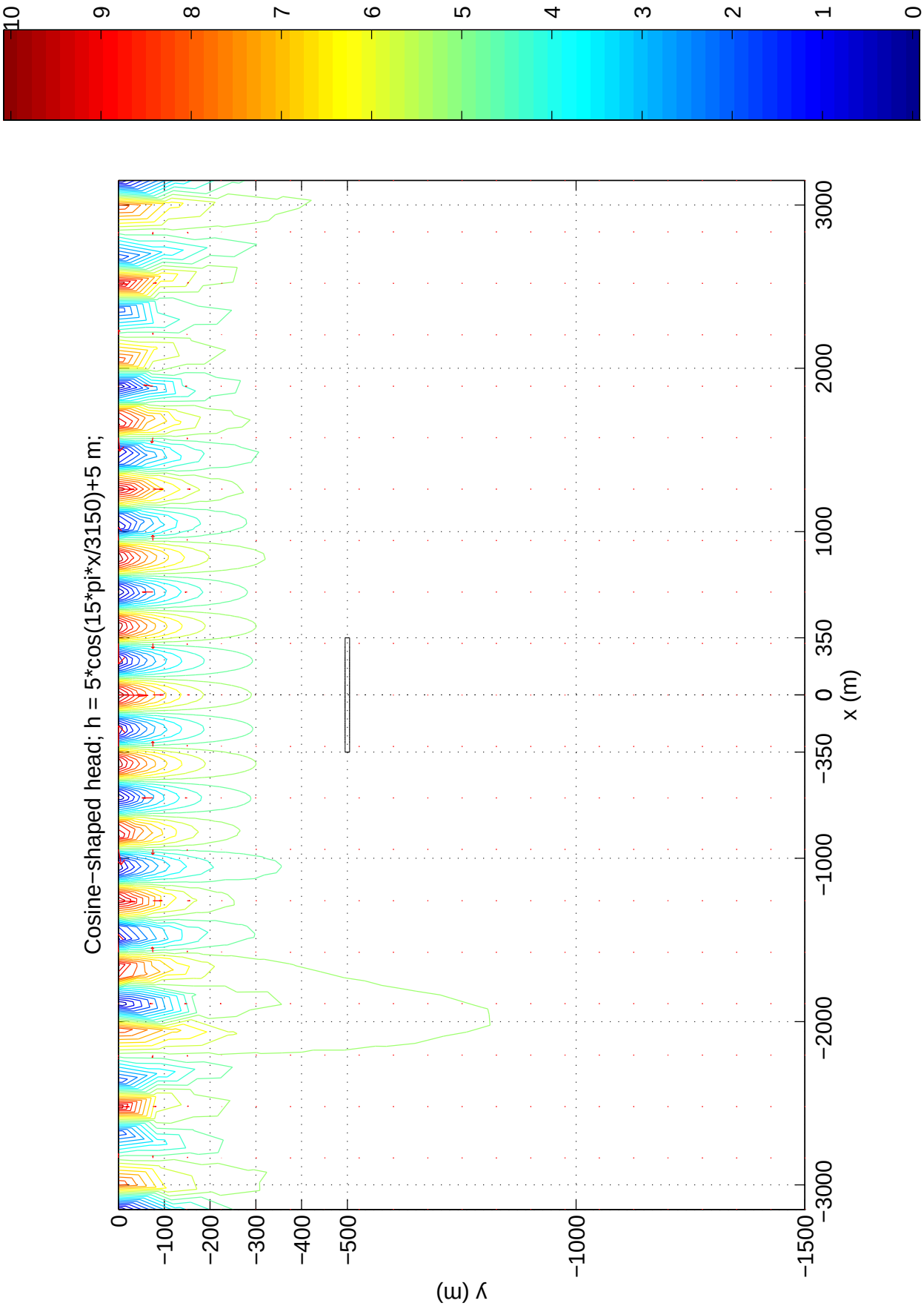

APPENDIX 20 STATE WITH A REPOSITORY: COSINE-SHAPED HEAD, THE SECOND VARIANT CASE, $K_{Rep} = 100 \cdot K_{500}$

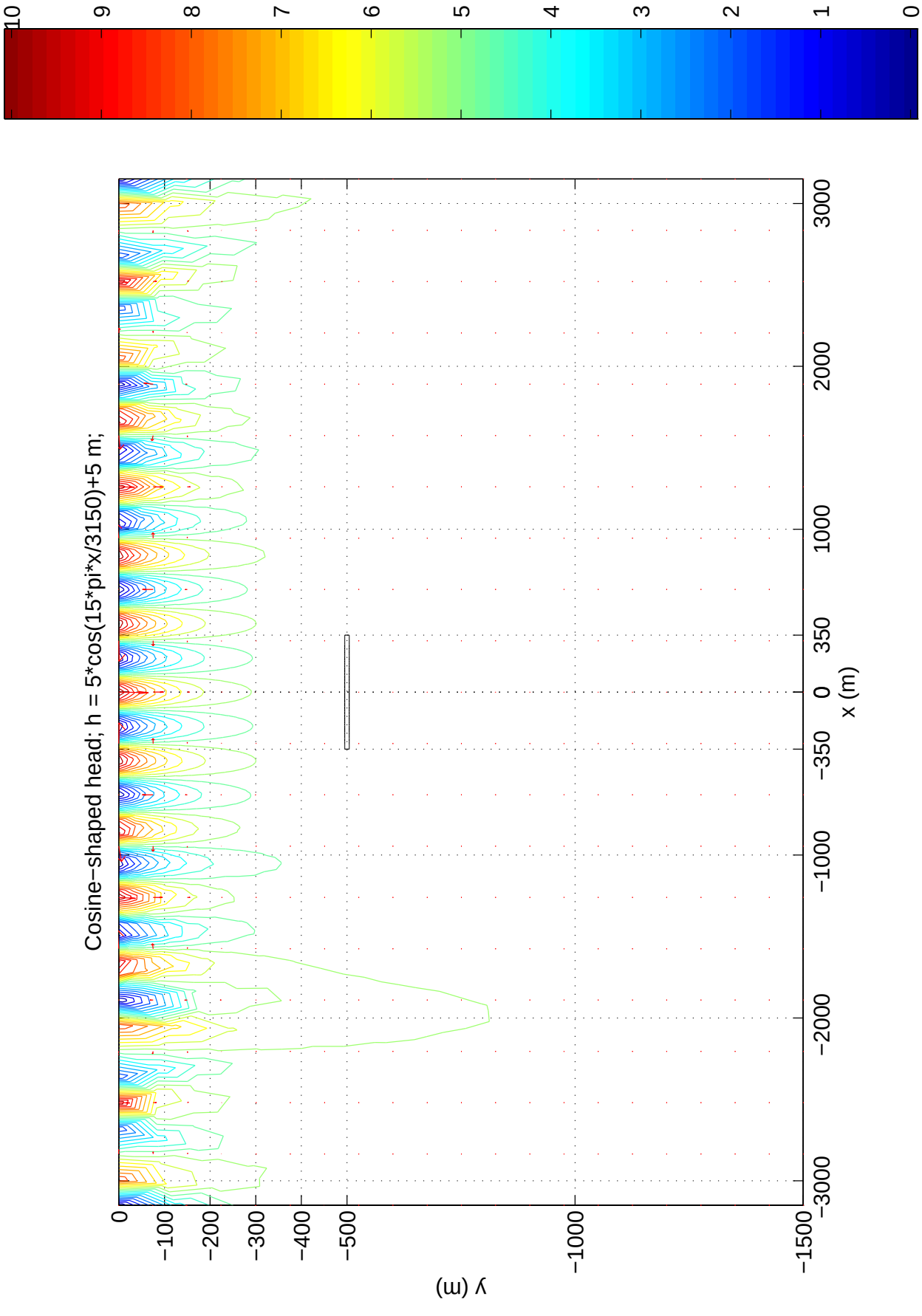

VARIATION OF THE FLOW FIELD AGAINST K_{Rep}: LINEAR HEAD, THE BASE CASE

APPENDIX 21

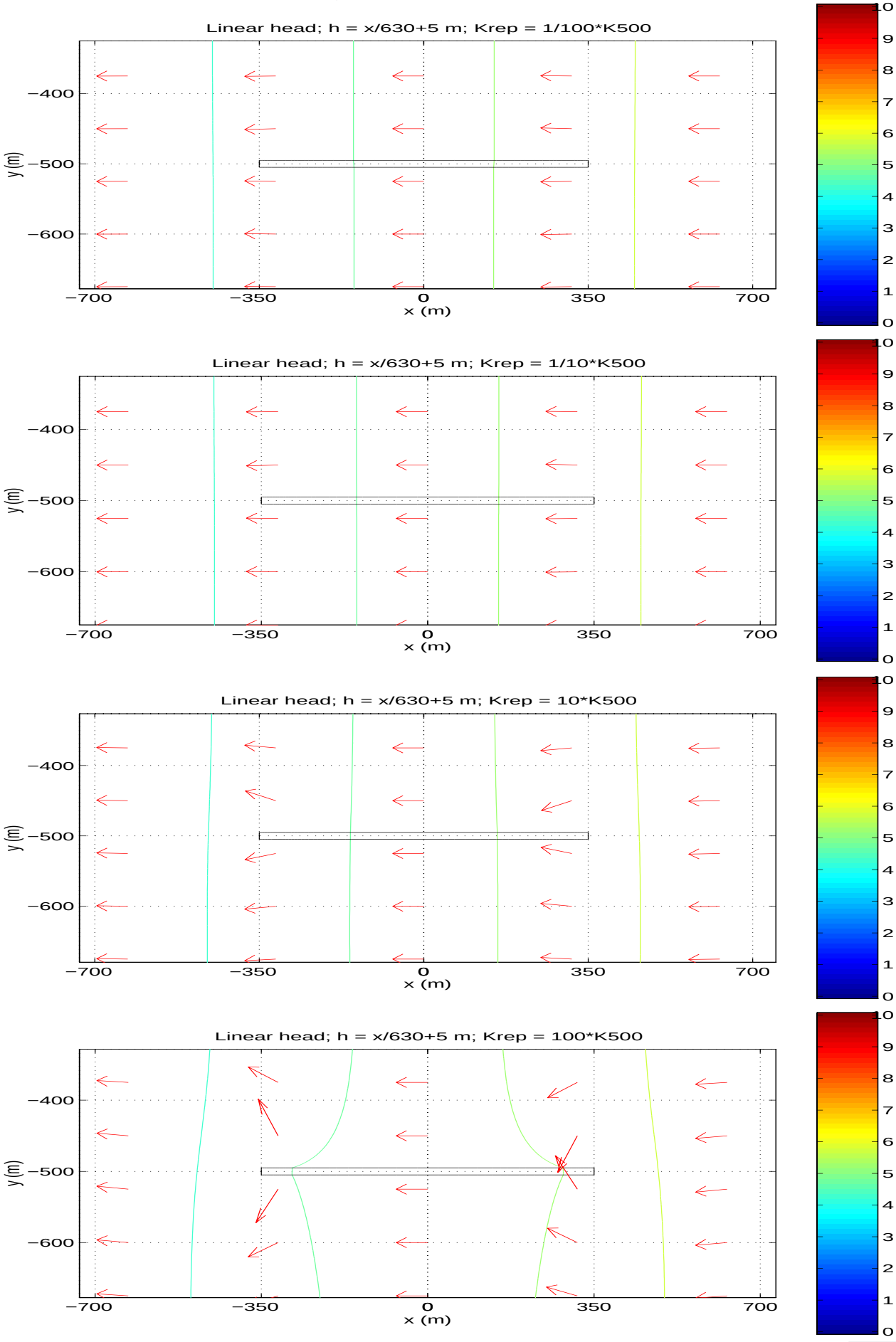

APPENDIX 22 VARIATION OF THE FLOW FIELD AGAINST K_{Rep}: PARABOLIC HEAD, THE BASE CASE

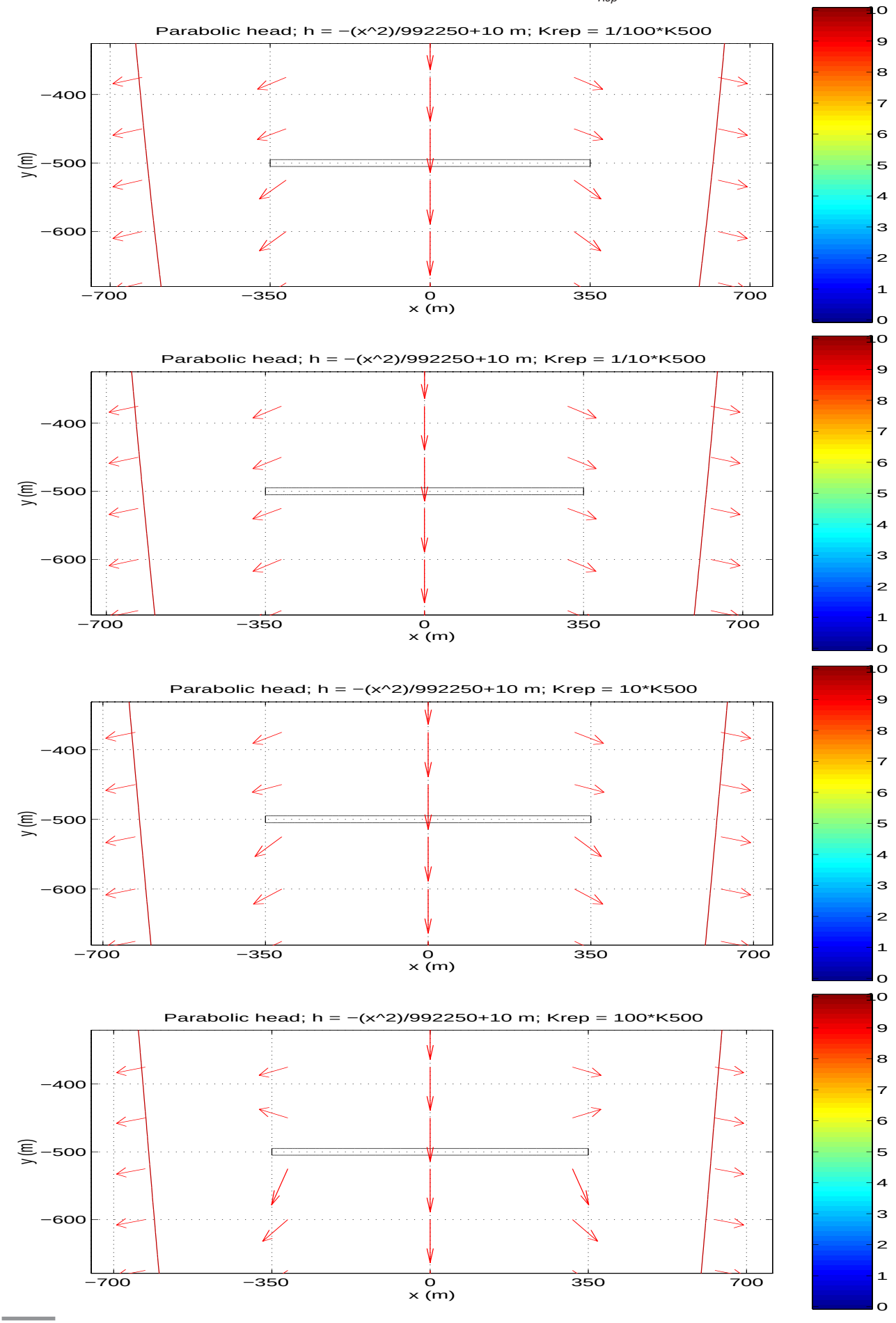

VARIATION OF THE FLOW FIELD AGAINST K_{Rep}: COSINE-SHAPED HEAD, THE BASE CASE

APPENDIX 23

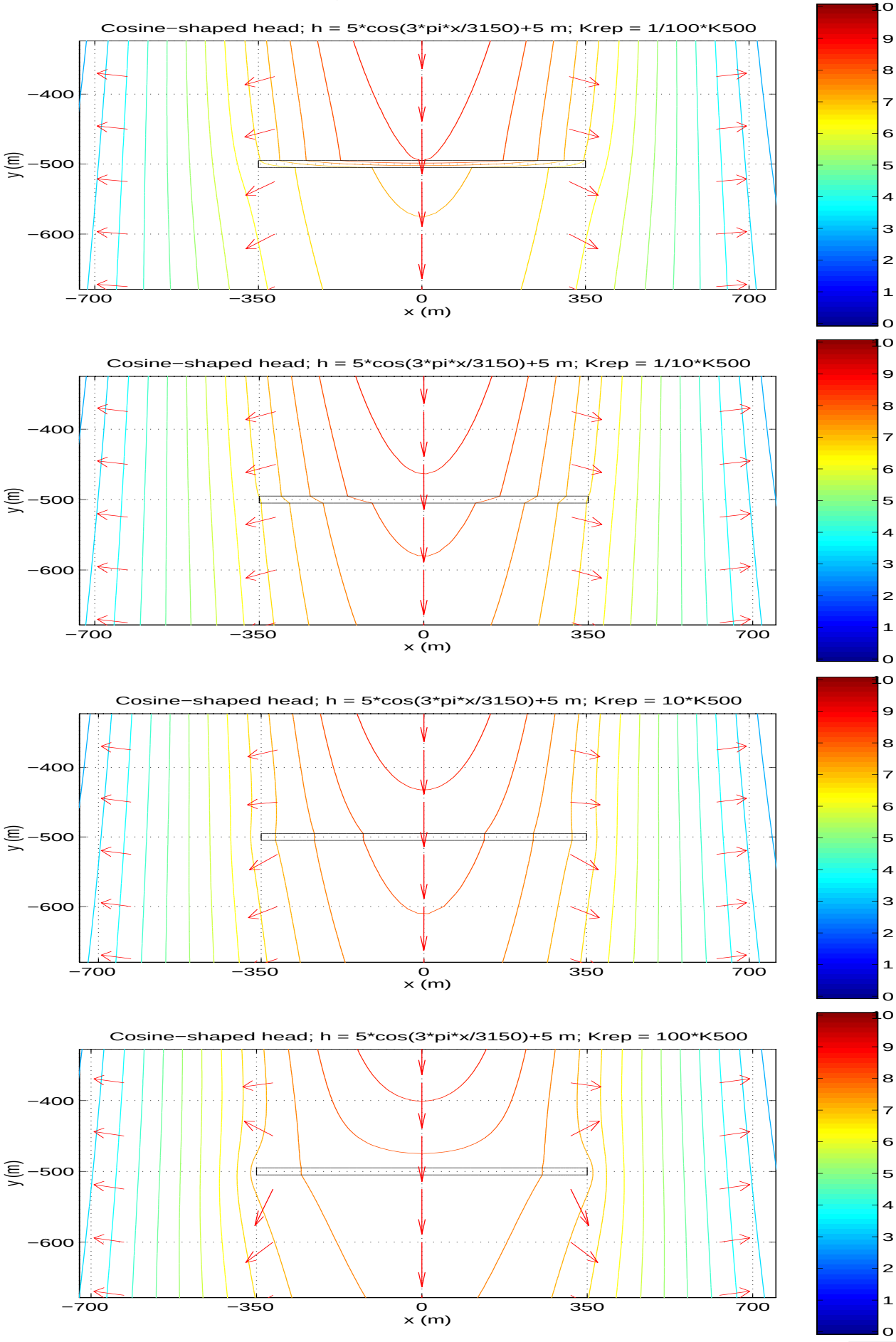

APPENDIX 24 VARIATION OF THE FLOW FIELD AGAINST K_{Rep}: COSINE-SHAPED HEAD, THE SECOND VARIANT CASE

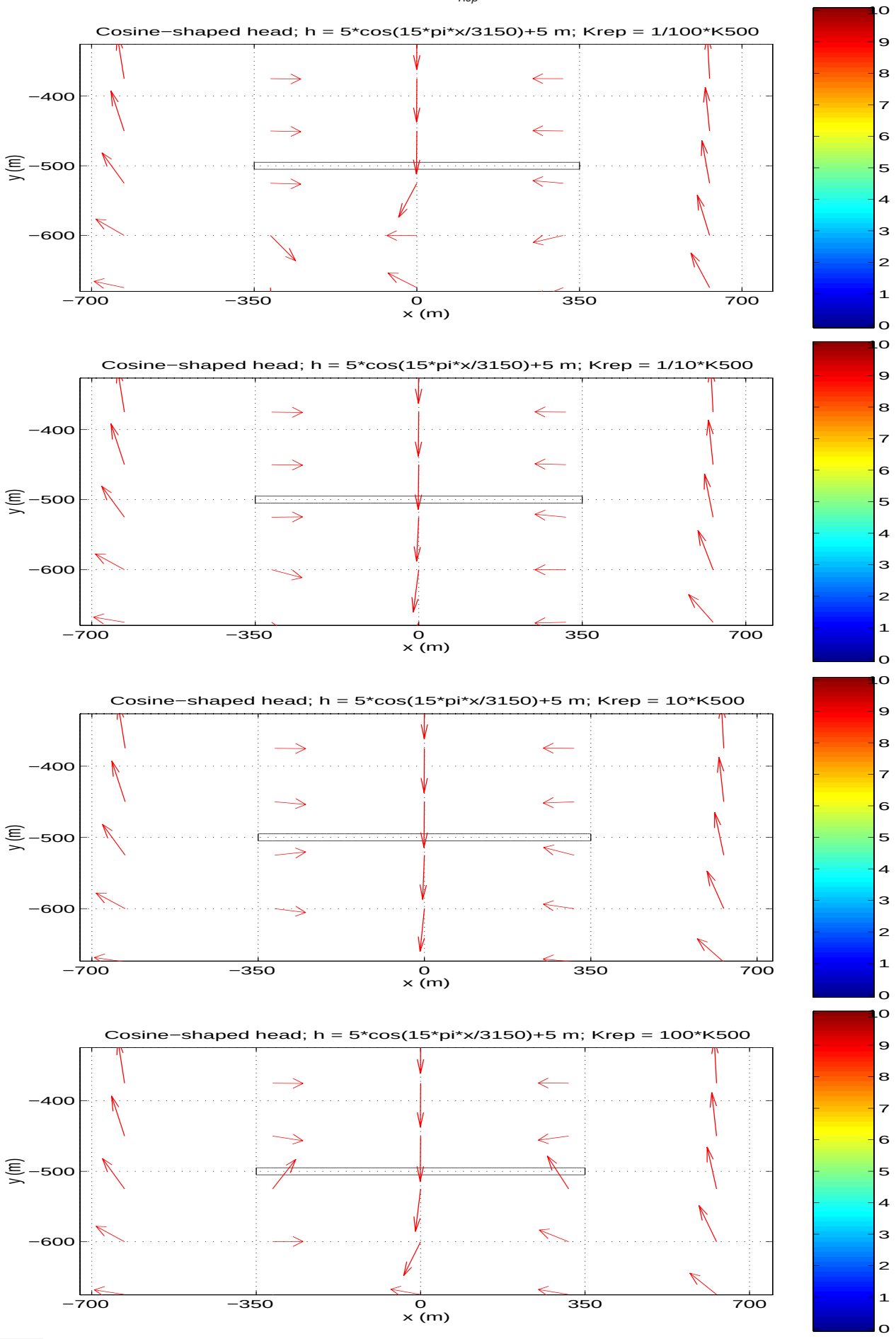

A SENSITIVITY CASE: PARABOLIC HEAD ON THE TOP,
EXPANSION OF THE SIDE BOUNDARIES TO X=±5000m

APPENDIX 25

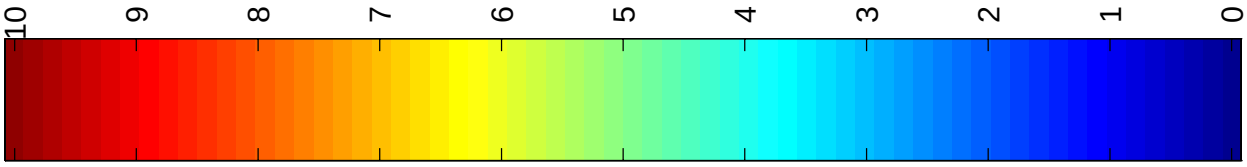

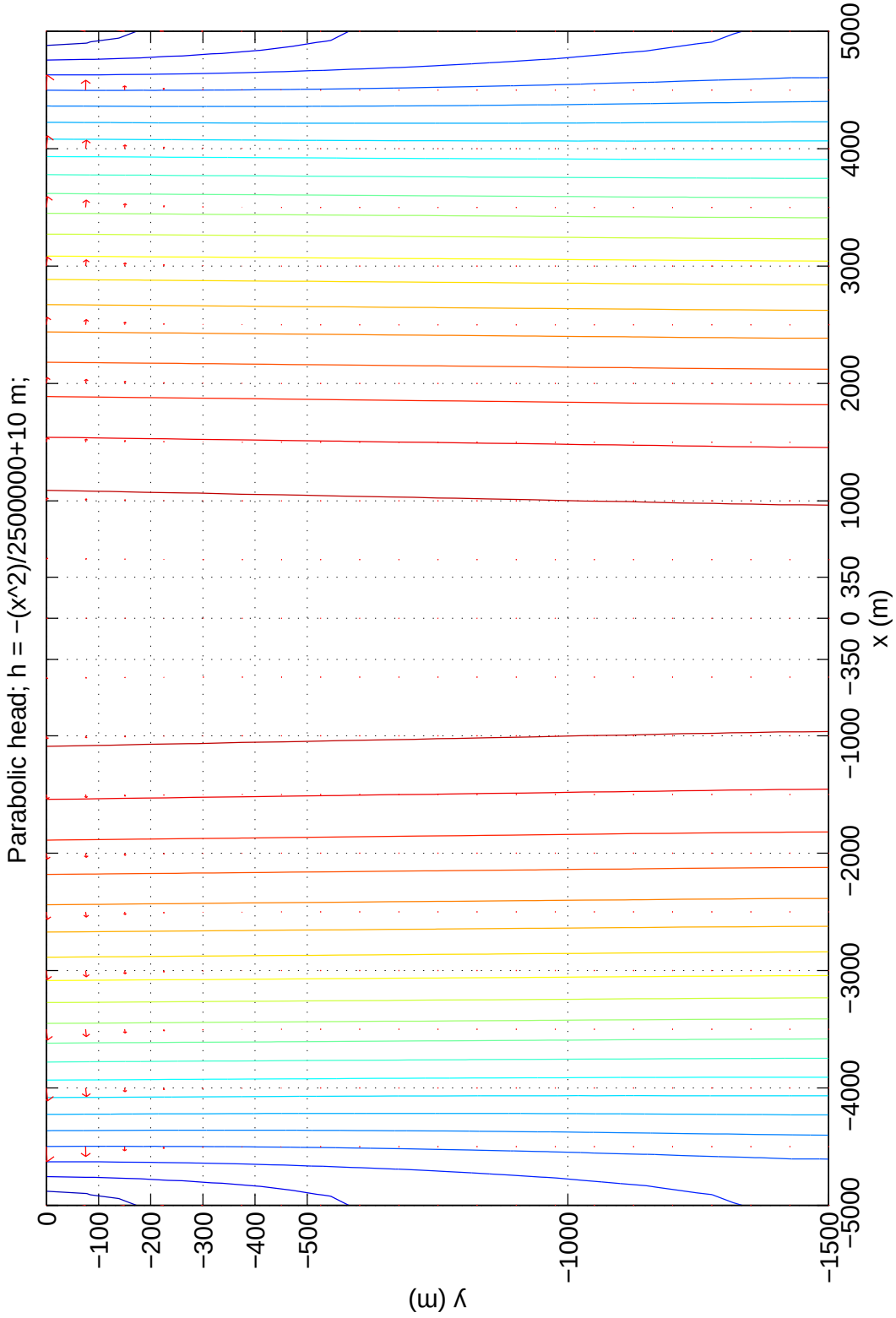

APPENDIX 26 A SENSITIVITY CASE: PARABOLIC HEAD ON THE TOP, LINEAR HEAD AT THE BOTTOM

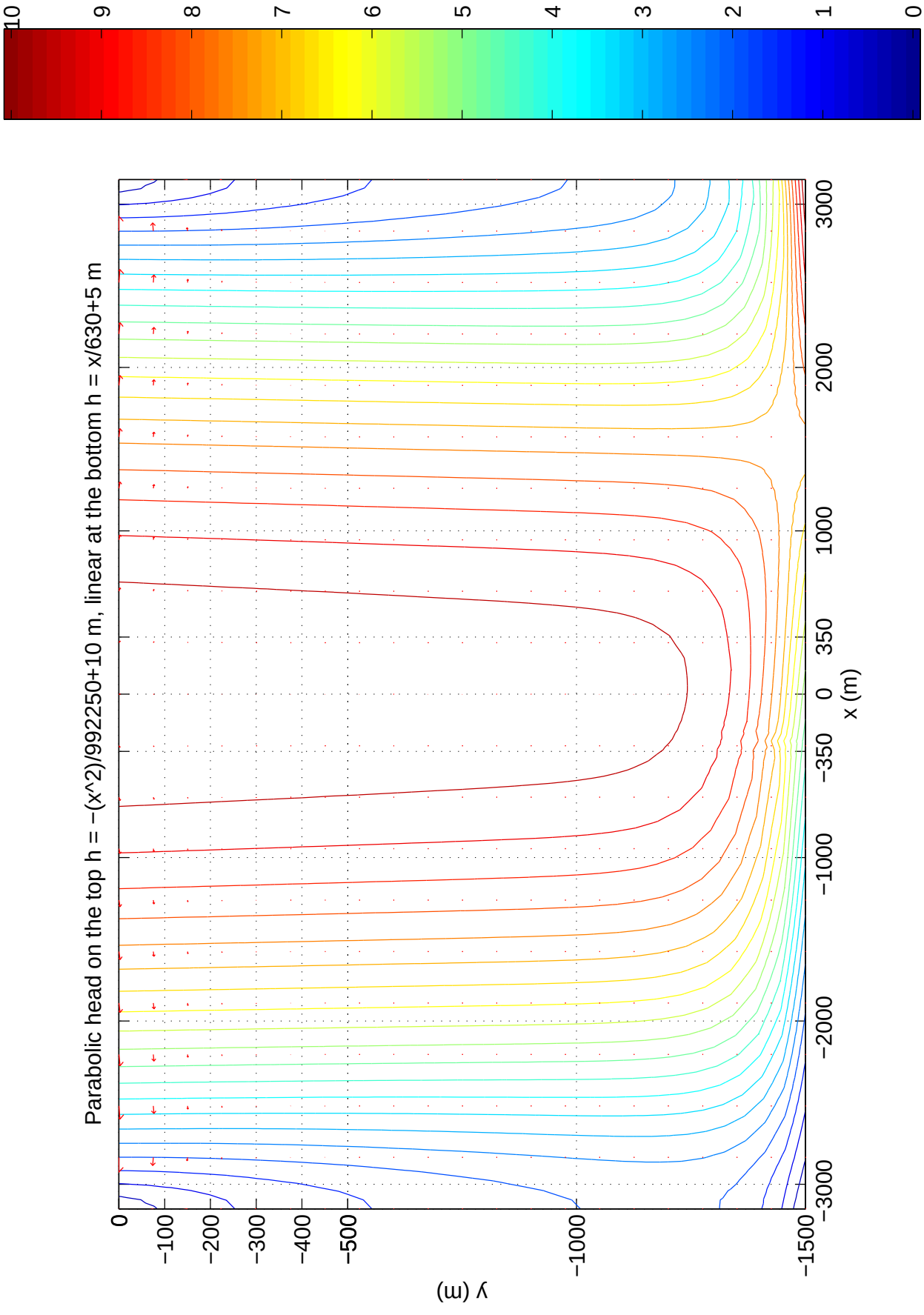

THE CALCULATION MESHES

APPENDIX 27